20. GEOCHEMISTRY OF BASALTS FROM DEEP SEA DRILLING PROJECT HOLES 556-564[1]

N. E. R. Drake, J. M. Rhodes, and L. K. Autio, Department of Geology and Geography, University of Massachusetts[2]

ABSTRACT

The nine holes (556–564) drilled during DSDP Leg 82 in a region west and southwest of the Azores Platform (Fig. 1) exhibit a wide variety of chemical compositions that indicate a complex petrogenetic history involving crystal fractionation, magma mixing, complex melting, and mantle heterogeneity. The major element chemistry of each hole except Hole 557 is typical of mid-ocean ridge basalts (MORBs), whereas the trace element and rare earth element (REE) abundances and ratios are more variable, and show that both depleted Type I and enriched Type II basalts have been erupted in the region.

Hole 556 (30–34 Ma), located near a flow line through the Azores Triple Junction, contains typically depleted basalts, whereas Hole 557 (18 Ma), located near the same flow line but closer to the Azores Platform, is a highly enriched FeTi basalt, indicating that the Azores hot-spot anomaly has existed in its present configuration for at least 18 Ma, but less than 30–34 Ma.

Hole 558 (34–37 Ma), located near a flow line through the FAMOUS and Leg 37 sites, includes both Type I and II basalts. Although the differences in Zr/Nb and light REE/heavy REE ratios imply different mantle sources, the $(La/Ce)_{ch}$ (>1) and Nd isotopic ratios are almost the same, suggesting that the complex melting and pervasive, small-scale mantle heterogeneity may account for the variations in trace element and REE ratios observed in Hole 558 (and FAMOUS sites).

Farther south, Hole 559 (34–37 Ma), contains enriched Type II basalts, whereas Hole 561 (14–17 Ma), located further east near the same flow line, contains Type I and II basalts. In this case, the $(La/Ce)_{ch}$ and Nd isotopic ratios are different, indicating two distinct mantle sources. Again, the existence along the same flow line of two holes exhibiting such different chemistry suggests that mantle heterogeneity may exist on a more pervasive and transient smaller scale. (Hole 560 was not sampled for this study because the single basalt clast recovered was used for shipboard analysis.)

All of the remaining three holes (562, 563, 564), located along a flow line about 100 km south of the Hayes Fracture Zone (33°N), contain only depleted Type I basalts.

The contrast in chemical compositions suggests that the Hayes Fracture Zone may act as a "domain" boundary between an area of fairly homogeneous, depleted Type I basalts to the south (Holes 562–564) and a region of complex, highly variable basalts to the north near the Azores hot-spot anomaly (Holes 556–561).

INTRODUCTION

During DSDP Leg 82, nine holes (556–564) were drilled near several spreading flow lines perpendicular to the Mid-Atlantic Ridge in a region west and southwest of the Azores Platform (Fig. 1). The northern flow lines are on either side of the Pico Fracture Zone and pass through the Azores Triple Junction (Holes 556 and 557) and the FAMOUS and Leg 37 sites (Hole 558). The southern flow lines straddle the Hayes Fracture Zone (Holes 559–561 and 562–564) 650 km south of the Azores Triple Junction. Drilling perpendicular to the ridge axis in crust aged 14–18 Ma (Anomalies 5–6) and 30–37 Ma (Anomalies 12–13) provided an opportunity to examine geochemical changes with time at a particular ridge segment. Figure 1 shows the position of the drill sites and summarizes the geochemical characteristics of the basalts from each hole. No analyses from Hole 560 are included because only one basalt clast was recovered, which was used for shipboard analysis. Further details on locations and recovery are given in the site chapters of this volume.

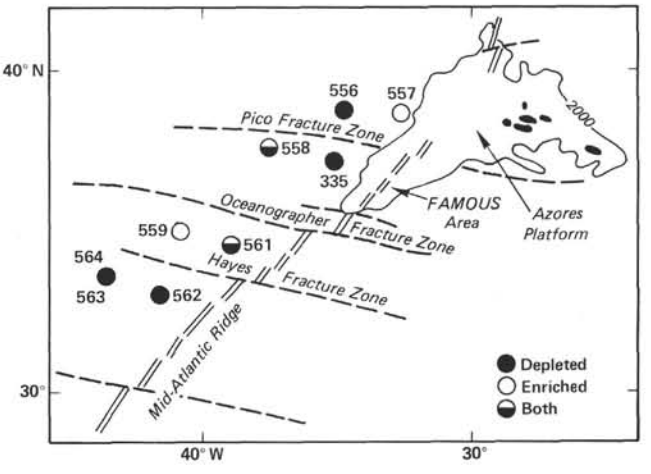

Figure 1. Location and chemical characteristics of basalts sampled on DSDP Leg 82.

The task of this study was to examine geochemical variations over the past 35 Ma in order to evaluate the roles played by crystal fractionation, magma mixing, complex melting, and large-scale or small-scale mantle heterogeneity in the petrogenesis of Leg 82 basaltic magmas. Such information is fundamental to a broader understanding of the composition and evolution of the oceanic mantle and crust.

[1] Bougault, H., Cande, S. C., et al., *Init. Repts. DSDP*, 82: Washington (U.S. Govt. Printing Office).

[2] Address: Department of Geology and Geography, University of Massachusetts, Amherst, Massachusetts 01003.

The 96 samples collected for this study were analyzed for major and trace elemental abundances by X-ray fluorescence (XRF) techniques (Appendixes A and B). Seven samples were selected for rare earth element (REE) analysis by instrumental neutron activation analysis (INAA) (Table 1). The chemical abundances and ratios were used to determine the chemical groups that in turn were used to evaluate the complex processes involved in basalt petrogenesis in the Leg 82 area. The geochemical data were also used to examine the important question of whether the Azores hot-spot anomaly consists of a single mantle plume (Schilling, 1975) or represents sampling of pervasive, small-scale mantle veining (Hanson, 1977; Zindler et al., 1979). The role of fracture zones (in this case, the Hayes Fracture Zone at 33°N) as possible domain boundaries between regions of mantle with different chemical signatures was also considered (Melson and O'Hearn, 1979; Bougault and Treuil, 1980).

Throughout the text, tables, figures, and appendixes we have used our own simplified sample numbering system. The first part of the number refers to the hole number (556–564) and the second part represents the samples in order of increasing depth within basement (i.e., the number 1 refers to the sample nearest the top of each hole). The DSDP designation for each sample can be found in the second to fourth rows at the top of Appendix A, Tables 1–7, which list all of the major and trace element abundances for each sample by hole number in order of increasing depth within basement.

METHODS

Samples were crushed in a tungsten carbide shatterbox at the Ronald B. Gilmore X-Ray Facility in the Department of Geology and Geography at the University of Massachusetts in Amherst. The major element data were obtained by XRF on fused glass disks, prepared by fusing the sample with a lanthanum-bearing lithium tetraborate flux (Norrish and Hutton, 1969). The trace elements (Rb, Sr, Y, Ga, Zr, Nb, Zn, Ni, Cr, and V) were determined by XRF analysis on pressed powder pellets. Corrections were made for nonlinear backgrounds, tube contamination, and interelement interferences (Norrish and Chappell, 1967). Corrections for matrix effects were based on a modification of the Compton scattering method (Reynolds, 1967). Additional trace element and REE data (La, Ce, Nd, Sm, Eu, Yb, Lu, Hf, Sc) (Table 1) were obtained by INAA in Fred Frey's laboratory at the Center for Geoalchemy in the Department of Earth and Planetary sciences at the Massachusetts Institute of Technology, by the methods of Jacobs and others (1977).

Average values for BCR-1 analyzed as an unknown by XRF are given in Table 2 with one standard deviation. Each element was analyzed twice for each sample. Error values labeled Leg 82 in Table 2 are based on these replicate analyses and apply directly to the Leg 82 basalts under the given operating conditions. The values were calculated using the formula:

$$s = \sqrt{\Sigma(x - \bar{x})^2/(n - 1)},$$

where x and $\bar{x}$ are observation and mean for replicate analyses of the same element in a single sample and n is the number of samples analyzed.

Mg′-values were calculated as molecular $Mg/(Mg + Fe^{2+})$, where molecular Fe has been proportioned as $Fe^{3+}/(Fe^{2+} + Fe^{3+}) = 0.1$ (Basaltic Volcanism Study Project, 1981). Fe_2O_3* and FeO* refer to total Fe expressed as Fe^{3+} or Fe^{2+}, respectively. Major elements are expressed as weight percent (wt.%) and trace elements in parts per million (ppm).

BASALT CHEMISTRY

Hole 556

Hole 556 is located near Anomaly 12 (30–34 Ma) about 80 km north of the Pico Fracture Zone on a flow line extending through the Azores Triple Junction (Fig. 1). The 16 basalt samples analyzed from 177 m of basement may be classified as two distinct, but stratigraphically interlayered basalt types. Group I is the more primitive of the two, with moderately high MgO (7.4 wt.%) and CaO (13.3 wt.%) contents, Mg′-values (0.66), and CaO/Al_2O_3 ratios (0.83) (Appendix A, Table 1; Appendix B, Table 1; Figs. 2–4). Ni (100 ppm) and Cr (340 ppm) contents are the lowest of all Leg 82 basalts and the Sr (99 ppm) contents are relatively low also (Figs. 5, 6). Incompatible element abundances, TiO_2 (1 wt.%), Zr (48 ppm), Y (22 ppm), and Nb (1.8 ppm) as well as Zr/Y ratios (2.5) (Fig. 7), are low relative to other ocean-floor basalts (Melson et al., 1977; Basaltic Volcanism Study Project, 1981).

Within Group I, two subgroups can be recognized; IA (556-1, 2, 7, 8, 9, 11, 13–16) and IB (556-10, 12, 17). Subgroup IA has lower Ni (99 versus 110 ppm) contents, Mg′-values (0.64 versus 0.67), and CaO/Al_2O_3 ratios

Table 1. Rare earth element and trace element abundances (ppm) in selected Leg 82 basalts.

Univ. Mass. sample number	558-1	558-2	558-7	558-13	561-2	561-6	563-2	ML-76	NB-STD	N
Hole	558	558	558	558	561					
Core-Section	27-3	28-1	33-2	38-1	1-1	2-2	24-1			
(interval in cm)	112–114	55–58	144–147	97–99	4–9	82–84	22–25			
Sub-bottom depth (m)	409.13	415.07	462.46	505.48	411.57	416.83	366.24			
La	6.42	3.06	9.79	5.33	13.99	2.87	1.93	9.67	10.73	0.33
Ce	14.7	7.5	19.4	13.0	26.8	8.2	5.6	23.2	27.7	0.88
Nd	12.0	9.7	17.1	10.7	20.0	9.8	7.8	26.8	16.8	0.60
Sm	2.81	2.63	3.09	2.12	3.68	3.02	2.08	4.79	3.72	0.181
Eu	1.01	0.96	1.10	0.79	1.22	1.41	0.82	1.70	1.21	0.069
Yb	2.42	3.06	2.36	2.12	2.88	3.78	2.67	2.15	2.32	0.20
Lu	0.38	0.43	0.34	0.34	0.44	0.55	0.41	0.30	0.48	0.034
Sc	34.1	40.1	36.1	35.9	36.9	42.5	41.4	30.5	9.9	
Hf	1.97	1.70	2.01	1.50	2.20	2.10	1.37	3.43	5.76	
$(La/Ce)_{ch}$	1.16	1.09	1.35	1.09	1.39	0.93	0.92	1.11	1.02	
$(La/Sm)_{ch}$	1.25	0.63	1.74	1.38	2.09	0.52	0.51	1.11	1.58	
$(La/Yb)_{ch}$	1.61	0.61	2.51	1.52	2.94	0.46	0.49	2.73	2.80	

Note: ch = chondrite-normalized ratios. ML-76 = Mauna Loa sample used as University of Massachusetts internal standard. NB-STD = M.I.T. internal standard. N refers to values used to normalize REE abundances to chondrites.

Table 2. Precision of whole-rock basalt chemistry analyses.

Elements	BCR-1	Leg 82 error
Major element (wt.%)		
SiO_2	54.51 (0.17)	(0.07)
TiO_2	2.25 (0.01)	(0.03)
Al_2O_3	13.52 (0.10)	(0.05)
Fe_2O_3*	13.36 (0.04)	(0.04)
MnO	0.19 (0.01)	(0.01)
MgO	3.33 (0.04)	(0.04)
CaO	6.93 (0.03)	(0.19)
Na_2O	3.30 (0.28)	(0.18)
K_2O	1.70 (0.01)	(0.01)
P_2O_5	0.38 (0.01)	(0.001)
Trace element (ppm)		
Rb	46.4 (0.3)	(0.20)
Sr	326 (1)	(0.58)
Y	33.5 (0.3)	(0.28)
Ga	22.2 (0.6)	(1.49)
Zr	194.5 (1.8)	(0.55)
Nb	12.5 (0.4)	(0.46)
Zn	128 (2)	(0.56)
Ni	22.8 (9.7)	(6.60)
Cr	5.7 (1.4)	(1.28)
V	360 (4)	(2.39)

Note: BCR-1 is a U.S.G.S. standard analyzed with every X-ray fluorescence run. Mean and 1 standard deviation (expressed in wt.% or ppm) are given. The column labeled Leg 82 error refers to the precision of analysis at the Leg 82 concentrations (see text) and is given as 1 standard deviation.

(0.83 versus 0.87), along with higher incompatible element abundances, TiO_2 (1.02 versus 0.86 wt.%), Zr (58 versus 48 ppm), and Y (23 versus 20 ppm), than Subgroup IB. However, the Sr (99 versus 100 ppm) content is the same for both subgroups (Fig. 6). The three samples from Subgroup IB and one sample from Subgroup IA (556-7) are unusually high in CaO (14 wt.%) (Fig. 3) for ocean-floor basalts (Melson et al., 1977; Basaltic Volcanism Study Project, 1981). These samples have few or no phenocrysts and no obvious carbonate veining or alteration.

Group II, consisting of four samples (556-3 through 556-6) has lower MgO (6.75 wt.%), CaO (11.7 wt.%), Ni (89 ppm), and Cr (250 ppm) contents, Mg′-values (0.58), and CaO/Al_2O_3 ratios (0.70), along with greater Zr/Y ratios (2.9) and incompatible element abundances—TiO_2 (1.45 wt.%), Zr (90 ppm), Nb (2.5 ppm), and Y (30 ppm)—than Group I. Group II also contains 100 ppm of Sr, the same amount as in Group I (Fig. 6).

Both groups have high Zr/Nb ratios (≥ 30) (Fig. 8) and are typical depleted Type I ocean-floor basalts according to the classification scheme of Bryan and others (1976). The compositional differences between the two groups coupled with a constant Zr/Nb ratio (Fig. 8) are qualitatively consistent with a comagmatic relationship between the two groups. Approximately 50% crystal fractionation involving olivine, plagioclase, and clinopyroxene is required to generate Group II basalts from Group I basalts.

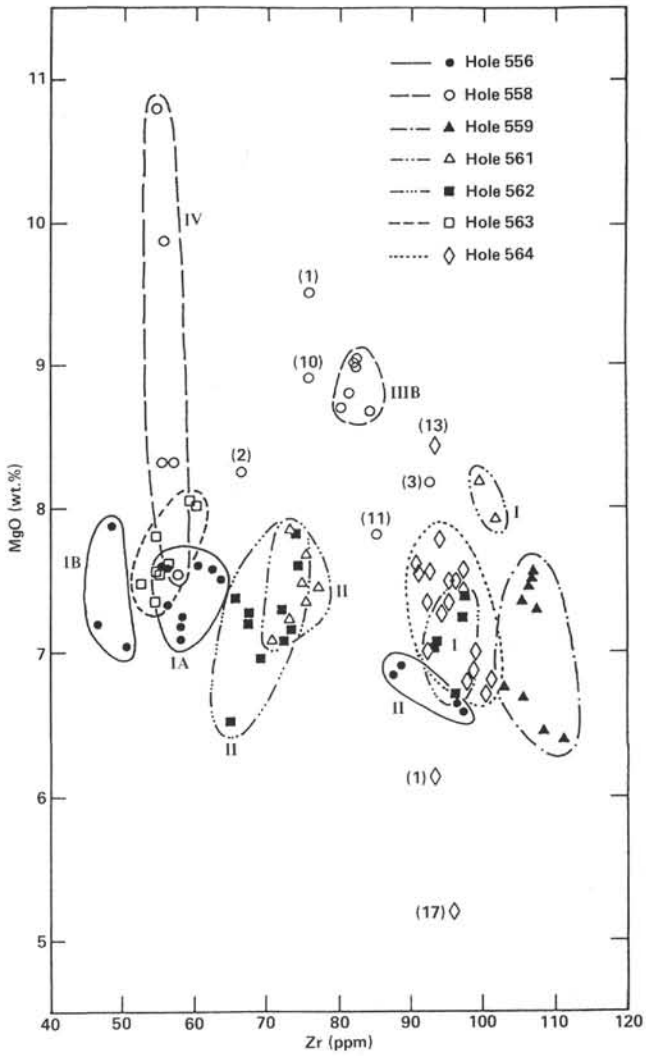

Figure 2. MgO versus Zr. Enclosures and Roman numerals refer to chemical groups within each hole. (All of the samples from Holes 559, 563, and 564 belong to Chemical Group I.) Arabic numbers in parentheses refer to the University of Massachusetts sample numbers (hole is indicated by shape of data point; see Appendix A tables for the DSDP sample designations for the samples).

It is unlikely, however, that this process is one of simple crystal fractionation. First, the observed phenocryst assemblages of only plagioclase ± olivine are not consistent with fractionation dominated by clinopyroxene (as is suggested by chemical considerations). Second, the fact that Ni and Cr abundances are approximately the same for the two groups, each with different amounts of incompatible elements (Fig. 5), is consistent with the evolution of both groups from a common parental magma. Such inconsistencies may be explained by a combination of fractional crystallization and mixing of consanguineous magmas (Rhodes et al., 1979). This interpretation receives support from the repetitive interlayering of Groups I and II. It is also possible to interpret the geochemical differences in terms of variable degrees of partial melting of a common source (Langmuir et al., 1977; Wood, 1979). In this case, the more enriched

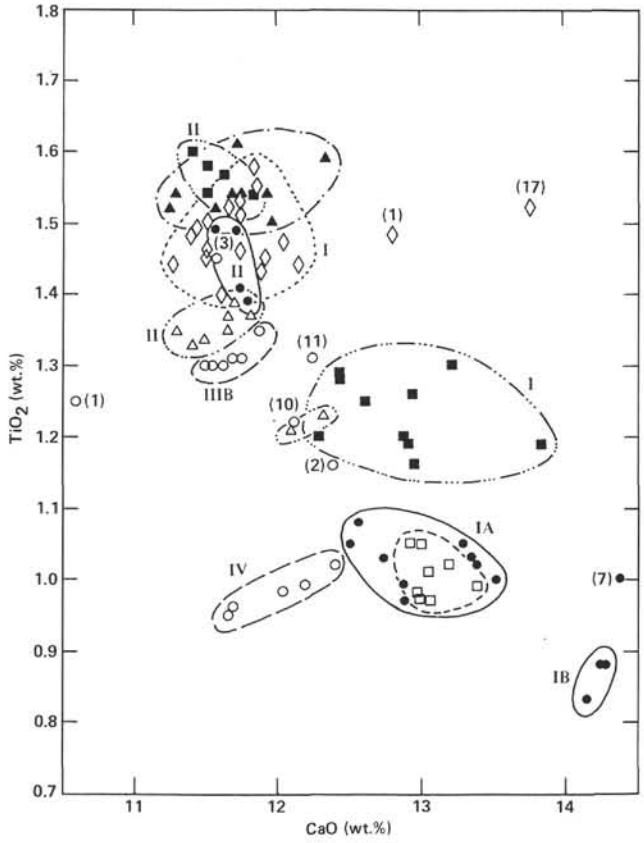

Figure 3. TiO_2 versus CaO. Symbols and enclosures are the same as in Figure 2.

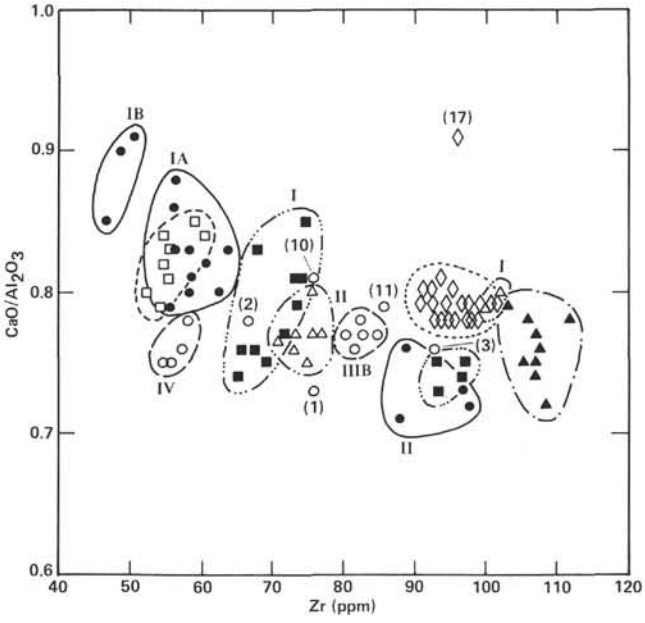

Figure 4. CaO/Al_2O_3 versus Zr. Symbols and enclosures are the same as in Figure 2.

Group II would have been produced by a lesser degree of melting. However, a plot of Sr versus Zr (Fig. 6) shows that both groups have about the same concentration of Sr (100 ppm) for very different concentrations of Zr. This relationship cannot be produced by different degrees of partial melting, but can be the result of fractionation/mixing processes.

Hole 557

Hole 557 is located near the same flow line as Hole 556, but near Anomaly 5D (18 Ma) closer to the Azores Triple Junction (Fig. 1). Only 3 m of basement were penetrated before the hole was abandoned because of inclement weather. Our one sample of this core, 557-1, falls into Group II of the shipboard studies (Site 557 chapter, this vol.). It has extremely high incompatible element abundances, TiO_2 (3.67 wt.%), Zr (216 ppm), Y (41 ppm), Nb (26 ppm) as well as high Fe_2O_3* (16.5 wt.%) and Sr (299 ppm), but very low MgO (5 wt.%), Ni (38 ppm), and Cr (19 ppm) abundances and a low Mg′-value (0.41) (Appendix A, Table 1). Thus, 557-1 is one of the more highly evolved or enriched basalts described to date from the ocean floor (Melson et al., 1977; Basaltic Volcanism Study Project, 1981). TiO_2 and FeO* abundances in 557-1 are similar to those of the enriched FeTi basalts of the Galapagos Spreading Center (Anderson et al., 1975; Schilling et al., 1976; Melson et al., 1977). Because of its extremely different abundances and ratios, Hole 557 data are not plotted on Figures 2–8.

The Zr/Nb ratio (8) and Zr/Y ratio (5) indicate that 557-1 is a Type II ocean-floor basalt (Bryan et al., 1976). The Zr/Y ratio is similar to that observed in Holes 407, 408, 410A, and 413 of DSDP Leg 49 (Tarney et al., 1979), but is higher than the Zr/Y ratios (2–4) observed in the other Leg 82 basalts (Fig. 7). It is likely that this basalt was derived from an unusually enriched source. If these basalts were derived from primitive Type II basalts similar to Group IV in Hole 558 (Appendix A, Table 2), the observed increase in incompatible element abundances would suggest as much as 70% crystal fractionation of olivine, plagioclase, and clinopyroxene. However, the lack of clinopyroxene phenocrysts and the close correlation of TiO_2 and Y abundances to other incompatible element abundances (indicating that clinopyroxene has not been a major fractionating phase) suggest that 557-1 is enriched by derivation from an enriched source rather than by evolution from a more typical ocean-floor basalt. CIPW norm calculations also indicate a more moderate state of evolution (557-1 is only slightly quartz normative).

Hole 558

Hole 558 is located between Anomalies 12 and 13 (34–37 Ma) about 50 km south of the Pico Fracture Zone on a flow line passing through DSDP Leg 37, Hole 335 (approximately 16.5 Ma), and the FAMOUS area (Recent) (Fig. 1). The 16 samples collected from 153.5 m of basement are compositionally the most complex of the Leg 82 basalts. The data indicate that four distinct basalt groups and two subgroups have been sampled (Appendix A, Table 2 and Appendix B, Table 2).

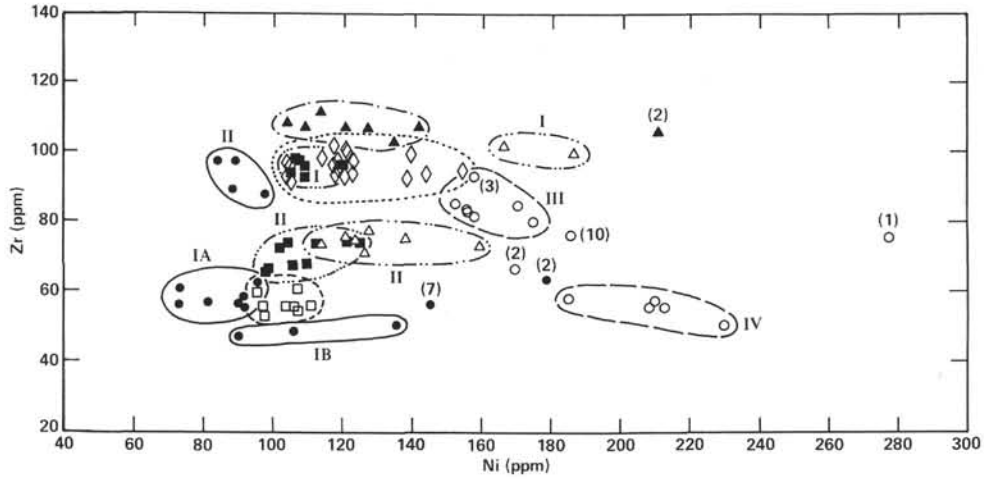

Figure 5. Zr versus Ni. Symbols and enclosures are the same as in Figure 2.

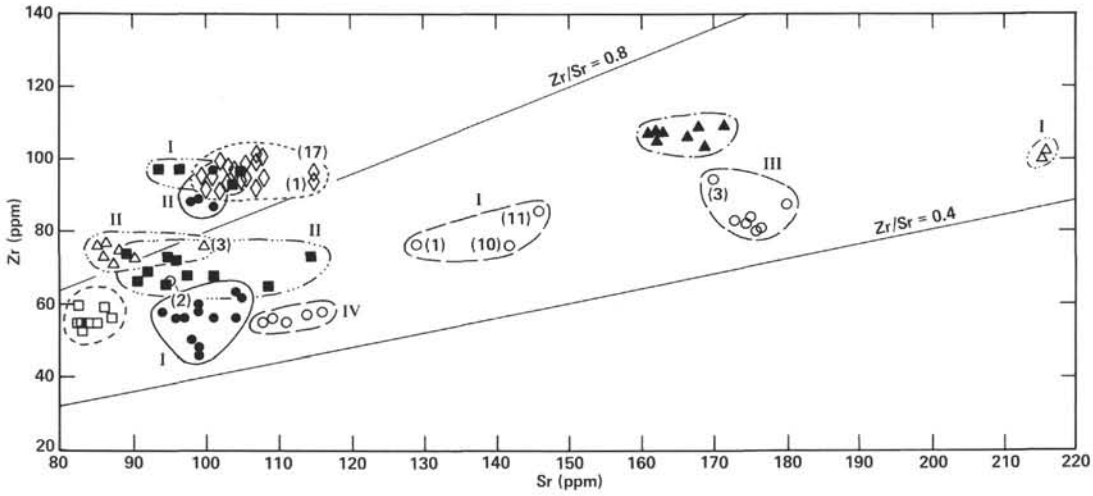

Figure 6. Zr versus Sr. Symbols and enclosures are the same as in Figure 2. Lines represent Zr/Sr ratios.

All of the chemical groups in this study correspond to shipboard groups except that three samples (558-1, 558-10, and 558-11) are included together in Group I because, although not stratigraphically contiguous, they have similar incompatible element abundances and ratios (Appendix A, Table 2; Figs. 7, 8).

Group I has moderate abundances of MgO (8.8 wt.%), CaO (11.7 wt.%), Sr (139 ppm), Ni (169 ppm) and Cr (344 ppm), Mg′-values (0.65), and CaO/Al_2O_3 ratios (0.77) (Appendix B, Table 2; Figs. 2–6). The abundances of incompatible elements are moderate as well, TiO_2 (1.26 wt.%), Zr (79 ppm), Nb (9.8 ppm), Y (23 ppm), as are the Zr/Y ratios (3.5) (Appendix B, Table 2; Fig. 7). Sample 558-1 has the highest MgO (9.5 wt.%), Ni (277 ppm), and Cr (510 ppm) abundances in Group I and the lowest CaO (10.6 wt.%) contents and CaO/Al_2O_3 ratio (0.73) (Appendix A, Table 2; Figs. 2–5), which could be due to olivine accumulation.

Group II, consisting of one sample, 558-2, also contains moderate abundances of major and trace elements; MgO (8.3 wt.%), CaO (12.4 wt.%), Ni (170 ppm), Cr (400 ppm), and CaO/Al_2O_3 ratio (0.78) (Appendix A, Table 2; Figs. 2–5). The Mg′-value is high (0.67), whereas the Sr content (95 ppm) is the lowest of all Hole 558 basalts (Fig. 6). Incompatible element abundances are somewhat low: TiO_2 (1.2 wt.%), Zr (66 ppm), Nb (2.3 ppm), and Y (26 ppm). The fact that Group II has the highest Y content and lowest Zr/Y ratio (2.6) for this hole (Fig. 7) precludes the possibility that Group II evolved from any of the other samples in Hole 558 by fractionation of clinopyroxene.

Group III consists of seven samples (558-3 through 558-9). It has the lowest CaO (11.6 wt.%), Ni (160 ppm), and Cr (368 ppm) and highest Sr (173 ppm), TiO_2 (1.35 wt.%), and Zr (88 ppm) abundances of all samples in Hole 558 (Appendix B, Table 2; Figs. 3, 5, 6). Yet the Ni and Cr contents are still fairly high, as are MgO contents (8.7 wt.%) and Mg′-values (0.66) (Figs. 2, 5). This suggests that the samples from Hole 558 are among the most primitive of Leg 82 basalts, even though Group III is the most evolved group at this site.

Within Group III are two subgroups. The single sample (558-3) in Subgroup IIIA differs from the other six samples in Subgroup IIIB; it has lower MgO (8.2 versus

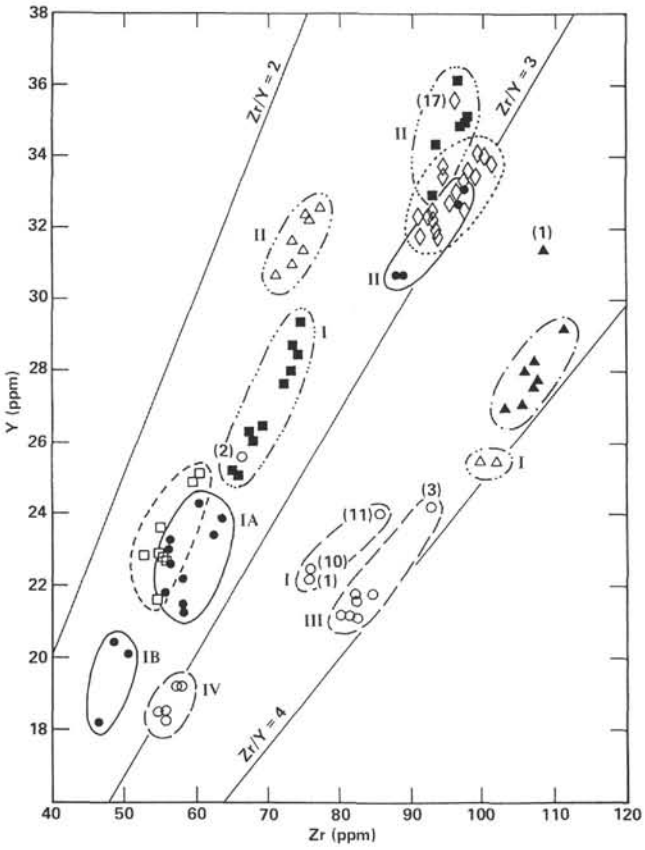

Figure 7. Y versus Zr. Symbols and enclosures are the same as in Figure 2. Lines represent constant Zr/Y ratios.

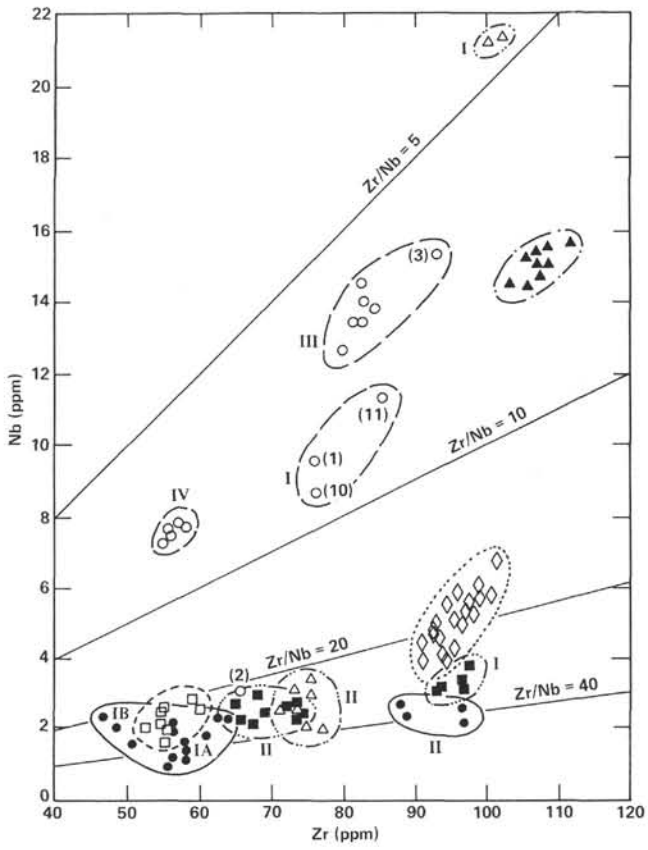

Figure 8. Nb versus Zr. Symbols and enclosures are the same as in Figure 2. Lines represent constant Zr/Nb ratios.

8.9 wt.%) contents and Mg′-values (0.64 versus 0.67) and greater abundances of incompatible elements, TiO_2 (1.45 versus 1.31 wt.%), Zr (93 versus 82 ppm), Nb (15.3 versus 13.6 ppm), and Y (24 versus 21 ppm) (Appendix B, Table 2). The similar CaO/Al_2O_3 ratios (0.77) and Ni (157 versus 162 ppm) and Cr (356 versus 379 ppm) contents for both subgroups (Figs. 4, 5) imply that Subgroups IIIA and IIIB may have either fractionated along closely parallel trends from slightly different parental magmas or undergone mixing during the fractionation process. Because IIIA contains about the same amount of Sr (170 versus 176 ppm) and more Zr than IIIB (Fig. 6), a melting trend is not possible, whereas mixing during fractionation is possible. Although the Zr/Y ratios are the same for both subgroups (3.8) (Fig. 7), the abundance of Y is higher for IIIA than IIIB, also supporting a more complex relationship than simple crystallization dominated by clinopyroxene fractionation.

Group IV, with five samples (558-12 through 558-16) has high MgO (7.5–10.8 wt.%), Ni (185–230 ppm) and Cr (442–482 ppm) contents, and Mg′-values (0.62–0.71), with moderate CaO (12.1 wt.%) and Sr (112 ppm) contents and CaO/Al_2O_3 ratios (0.76) (Appendix B, Table 2; Figs. 2–6). These basalts exhibit low incompatible element abundances; TiO_2 (<1 wt.%), Zr (55 ppm), Nb (7.6 ppm), and Y (19 ppm) and Zr/Y ratios (3.0) (Fig. 7). These abundances and ratios make Group IV the most primitive of the Leg 82 basalts. The primitive nature of Group IV basalts is also shown by the trends seen in Figures 2, 3, and 5 of Zr versus MgO, CaO, and Ni, respectively, which indicate olivine-controlled fractionation.

Within Group IV, Samples 558-13 and 558-16 are possible candidates for primary ocean-floor basalts. They have the highest abundances of MgO (10.8 and 9.9 wt.%), Ni (230 and 214 ppm) and Cr (449 and 441 ppm), and Mg′-values (0.71 and 0.69) of all Leg 82 basalts (except 558-1 for Ni) and low incompatible element abundances (Appendix A, Table 2). They are chemically similar to other proposed primary ocean-floor basalts such as those from DSDP Leg 3 (Frey et al., 1974), the FAMOUS area (Langmuir et al., 1977; White and Bryan, 1977), and the Mid-Atlantic Ridge at 45°N (Melson et al., 1977; Rhodes et al., 1979; Basaltic Volcanism Study Project, 1981).

It seems unlikely that the basalts from these four groups are comagmatic. Basalt samples from all four groups, which have comparable MgO and Ni abundances, Mg′-values, and CaO/Al_2O_3 ratios, have markedly different abundances of Zr and other incompatible elements (Figs. 2, 4, 5). In addition, these four chemical groups all have different Zr/Nb ratios (Fig. 8): Groups I, III, and IV have low values (8, 6, and 7.5, respectively), typical of Type II basalts (Bryan et al., 1976), but Group II is somewhat anomalous with a Zr/Nb ratio of about 20 (Fig. 8), similar to many basalts sampled on the Juan de Fuca Ridge (Liias and Rhodes, 1982).

REE data were obtained for four representative samples, one from each group (Table 1; Fig. 9A). Samples 558-1, 558-7, and 558-13 (Groups I, III, IV, respective-

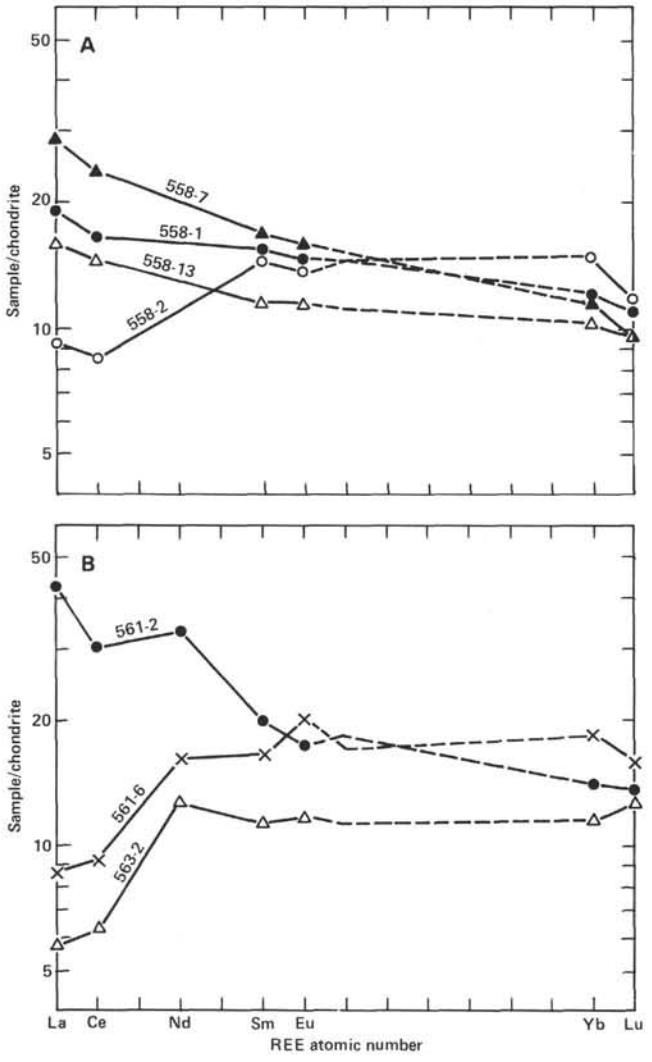

Figure 9. A. Chondrite-normalized rare earth element (REE) abundances for selected basalts in Hole 558. Sample numbers are the simplified numbers used in this study. Complete DSDP designations are located at the top of Appendix A, Table 2. B. Chondrite-normalized REE abundances for selected basalts in Holes 561 and 563. Sample numbers are the simplified numbers used for this study. Complete DSDP designations are located at the top of Appendix A, Tables 4 and 6.

ly) all show LREE-enriched patterns with chondrite-normalized (ch) ratios: $(La/Sm)_{ch} > 1$ (1.25–1.8) and $(La/Yb)_{ch} > 1$ (1.5–2.5) (Table 1). In marked contrast, Sample 558-2 (Group II) has a LREE-depleted pattern with $(La/Sm)_{ch} < 1$ (0.63) and $(La/Yb)_{ch} < 1$ (0.61). Although the $(La/Sm)_{ch}$ ratios are variable, the $(La/Ce)_{ch}$ ratios are >1 (1.09–1.35) for all four groups, similar to other basalts along this flow line, such as those from DSDP Leg 37 (Blanchard et al., 1976) and the FAMOUS area (Langmuir et al., 1977; White and Bryan, 1977).

Hole 559

Hole 559 is located between Anomalies 12 and 13 (34–37 Ma) midway between the Oceanographer and Hayes fracture zones (Fig. 1). All nine samples from the 63 m of basement are similar in composition (Appendix A, Table 3; Appendix B, Table 3) and compose a single chemical group consisting of enriched Type II basalts (Bryan et al., 1976) with typical Zr/Nb ratios (7–7.5) (Fig. 8). These basalts have some of the lowest CaO (11.7 wt.%) contents and CaO/Al_2O_3 ratios (0.76) and highest incompatible element abundances—TiO_2 (1.54 wt.%), Zr (107 ppm), Y (28 ppm), and Nb (15 ppm)—of all Leg 82 samples except 557-1 (Appendix A, Tables 1, 3; Appendix B, Table 3; Figs. 3, 4, 7, 8). However, the MgO (7.1 wt.%) and Ni (135 ppm) contents and the Mg′-value (0.59) are higher than expected relative to the concentration of incompatible elements (Figs. 2, 5).

The basalts from Hole 559 show stratigraphically interlayered variations in MgO, FeO*, and Mg′-values. Samples 559-2, 559-3, 559-5, 559-7, and 559-8 have lower MgO abundances (6.5 versus 7.5 wt.%) and Mg′-values (0.56 versus 0.62) and higher Fe_2O_3* (11.6 versus 10.5 wt.%) abundances than Samples 559-1, 559-4, 559-6, and 559-9 (Appendix B, Table 3; Fig. 2). This interlayering involving only the elements Mg and Fe could be the result of periodic replenishment of a multiply saturated magma by a more-primitive, olivine-rich melt (Rhodes et al., 1979). The relatively high Ni values (Fig. 5) also suggest that these basalts are enriched in olivine relative to other similarly evolved basalts (Basaltic Volcanism Study Project, 1981).

The incompatible element abundances (Appendix B, Table 3) are consistent with approximately 50% crystal fractionation from a more primitive Type II magma similar to the Group IV basalts sampled at Hole 558 (Appendix B, Table 2). Low CaO/Al_2O_3 ratios (0.76) (Fig. 4) coupled with high Zr/Y ratios (3.8) (Fig. 7) point towards clinopyroxene involvement in the fractionation process. However, clinopyroxene is notably absent from the observed phenocryst assemblage. The discrepancy between the chemistry and petrography, already encountered in Holes 556, 557, and 558, is a common problem for MORB (Dungan and Rhodes, 1978; Basaltic Volcanism Study Project, 1981) and points to a complex petrogenesis involving fractionation and mixing processes.

Sample 559-1 has the highest Y (31.6 ppm) abundance and the lowest Zr/Y ratio (3.43) of Hole 559 basalts (Fig. 7) and therefore could not have fractionated from compositions similar to the other samples in Hole 559. Possibly the observed anomalous behavior of 559-1 is a result of mantle heterogeneity or complex melting processes.

Hole 561

Hole 561 is located near Anomaly 5E (14–17 Ma) east of Hole 559 and along the same flow line (Fig. 1). The 15.1 m of basement is represented by nine samples that fall into two stratigraphically distinct groups. Group I is represented by two samples in the upper 0.7 m of the core, and Group II by seven samples in the lower 14.4 m. (Appendix A, Table 4; Appendix B, Table 4).

The upper basalts (Group I) have greater MgO (8.1 versus 7.4 wt.%), CaO (12.2 versus 11.6 wt.%), Sr (215 versus 89 ppm), and Ni (176 versus 130 ppm) abun-

dances and Mg′-values (0.64 versus 0.59), but lower Fe_2O_3* contents (9.9 versus 11.5 wt.%) than the lower basalts (Group II).

Zr/Nb ratios are strikingly different for the two groups (Fig. 8). Group I, with low Zr/Nb ratios (<5), is a Type II basalt (Bryan et al., 1976), whereas Group II, which has higher Zr/Nb ratios (>25), is a Type I basalt. Two representative samples, 561-2 of Group I and 561-6 of Group II, were analyzed for REE (Table 1; Fig. 9B). Sample 561-2 is LREE enriched with chondrite-normalized ratios >1: $(La/Ce)_{ch}$ = 1.39, $(La/Sm)_{ch}$ = 2.09, and $(La/Yb)_{ch}$ = 2.94, all typical of LREE-enriched Type II ocean-floor basalts (Bryan et al., 1976). Sample 561-6, however, is a typical LREE-depleted Type I ocean-floor basalt, with chondrite-normalized ratios <1: $(La/Ce)_{ch}$ = 0.93, $(La/Sm)_{ch}$ = 0.52, and $(La/Yb)_{ch}$ = 0.46. This is in marked contrast to Hole 558 where the $(La/Ce)_{ch}$ ratio is fairly constant (>1) even though variations in the $(La/Sm)_{ch}$ ratios occur between Groups I and II (Table 1; Figs. 9A and 9B).

Group I has greater Zr/Y (4 versus 2.5) (Fig. 7) and Zr/TiO_2 (90 versus 55) ratios and Zr abundances (100 versus 75 ppm) than Group II, but lower Y (25 versus 30 ppm) and TiO_2 (1.2 versus 1.4 wt.%) contents (Appendix B, Table 4). These features, combined with the different Zr/Nb and $(La/Ce)_{ch}$ ratios, suggest that two distinct parental magmas are required, which is further supported by the two trends of decreasing Ni abundances at different Zr concentrations (Fig. 5). The Nd isotopic ratios (Jenner et al., this vol.) are distinctly different for the two groups and also indicate two distinct sources.

Hole 562

Hole 562 is located in 14–17 Ma crust near Anomaly 5D along a flow line about 100 km south of the Hayes Fracture Zone (Fig. 1). Sixteen samples from 90.1 m of basement fall into two stratigraphically separated chemical groups (Appendix A, Table 5; Appendix B, Table 5). Group I is represented by six samples in the upper 49.5 m of core and Group II by ten samples in the lower 40.6 m. Both groups have Zr/Nb ratios >20 (Fig. 8) and are depleted Type I MORB (Bryan et al., 1976).

Group I, which is higher stratigraphically and therefore more recently erupted, is the more evolved of the two groups. It has lower CaO (11.6 versus 12.9 wt.%) and MgO (7.0 versus 7.2 wt.%) abundances, CaO/Al_2O_3 ratios (0.74 versus 0.79), and Mg′-values (0.57 versus 0.61) (Figs. 2–4). Abundances of incompatible elements, TiO_2 (1.6 versus 1.2 wt.%), Zr (96 versus 70 ppm), and Y (35 versus 27 ppm), and Zr/Y ratios (2.8 versus 2.6) (Fig. 7), are correspondingly higher in Group I than Group II. However, Ni (109 versus 108 ppm), Cr (231 versus 257 ppm), and Sr (100 versus 98 ppm) abundances are similar for the two groups (Figs. 5, 6).

Within Group II, Al_2O_3 increases and CaO/Al_2O_3 ratios decrease with decreasing Zr (Fig. 4) as a consequence of plagioclase accumulation. The most plagioclase phyric samples occur at the high Al_2O_3–low Zr end of the trend.

The above-noted increase in incompatible elements is consistent with about 22–25% crystal fractionation. The small increase in Zr/Y ratios from Group II to Group I and the fact that TiO_2 and Y are behaving less incompatibly than Zr and Nb indicate clinopyroxene on the liquidus. Based on these relations and the trends shown in Figure 7, the two groups could be comagmatic, with Group I basalts having evolved from a magma with Group II composition.

However, as in Hole 556, the Ni abundances for the two groups are approximately the same, although abundances of ZR (and other incompatible elements) are different (Appendix B, Table 5; Fig. 5). These Ni-Zr relationships for the two basalt groups may be the result of the mixing of consanguineous magmas (Rhodes et al., 1979), or alternatively, fractionation of distinct parental magmas produced by slightly different amounts of melting of a similar source. Once again, the two chemical groups have the same Sr concentrations with different Zr concentrations (Fig. 6). This precludes partial melting and supports the idea of fractionation and magma mixing as proposed for Holes 556 and 558 in this study.

Hole 563

Hole 563 is located near Anomaly 13 (34–37 Ma) west of Hole 562 and near the same flow line south of the Hayes Fracture Zone (Fig. 1). The eight samples taken from 18 m of basement compose a single chemical group. These samples have the following major and trace element abundances: MgO (7.7 wt.%), CaO (13 wt.%), Fe_2O_3* (10.1 wt.%), Ni (103 ppm), and Cr (239 ppm), Mg′-values (0.63), and CaO/Al_2O_3 ratios (0.8) (Appendix A, Table 6; Appendix B, Table 6). Abundances of Sr (84 ppm) and incompatible elements, TiO_2 (1 wt.%), Zr (50 ppm), Y (23 ppm), and Nb (2.3 ppm), and Zr/Y ratios (<2.5) are low.

As in Hole 559, the samples in Hole 563 show similar stratigraphically interlayered variations in MgO and Fe_2O_3* abundances and Mg′-values (Appendix A, Table 6; Fig. 2). Samples 563-1, 563-2, 563-4, 563-6, and 563-8 have lower MgO (7.5 versus 8 wt.%) abundances and Mg′-values (0.62 versus 0.64) and greater Fe_2O_3* (10.3 versus 9.9 wt.%) abundances than Samples 563-3, 563-5, and 563-7. The interlayered fluctuations in these elements could imply periodic replenishment of an evolving magma reservoir by more primitive melts (Rhodes et al., 1979).

As in Hole 562, plagioclase accumulation is indicated both petrographically and chemically. In samples with such accumulations, MgO and Zr abundances and CaO/Al_2O_3 ratios decrease whereas Al_2O_3 increases with increasing amounts of plagioclase (Figs. 2, 4).

The compositional data (Appendix A, Table 6) indicate that Hole 563 contains some of the more primitive of the Leg 82 samples. Unlike most Leg 82 basalts, however, clinopyroxene fractionation does not appear to be important in the petrogenesis of Hole 563 basalts, an observation further supported by the Zr/Y ratios, which remain roughly constant (≤2.5) or decrease slightly with increasing Zr (Fig. 7).

One sample, 563-2, was analyzed for REE. It yielded chondrite-normalized ratios <1: $(La/Ce)_{ch}$ = 0.92, $(La/Sm)_{ch}$ = 0.51, and $(La/Yb)_{ch}$ = 0.49 (Table 1; Fig. 9B).

The resulting LREE-depleted pattern, along with Zr/Nb ratios >20 (Fig. 8), mark Hole 563 samples as depleted Type I basalts (Bryan et al., 1976). Similar results were obtained for other basalts collected south of the Hayes Fracture Zone.

Hole 564

Hole 564 is located near Anomaly 13 (34–37 Ma) south of the Hayes Fracture Zone, about 10 km north of Hole 563 (Fig. 1). Twenty samples were taken from 81 m of basement. These basalts exhibit high incompatible element abundances, TiO_2 (1.5 wt.%), Zr (96 ppm), Y (33 ppm), and Nb (5 ppm); low abundances of CaO (11.8 wt.%) and Fe_2O_3* (11.9 wt.%); and moderate MgO (7.2 wt.%) and Sr (105 ppm) contents, Mg′-values (0.57), and CaO/Al_2O_3 ratios (0.80) (Appendix A, Table 7; Appendix B, Table 7). These compositional characteristics suggest that Hole 564 basalts are fairly evolved, possibly with clinopyroxene on the liquidus.

Sample 564-17 deviates from the compositional relationships exhibited by the other basalts from this hole and may constitute a separate group or subgroup. Its distinctly lower MgO content (5.2 wt.%) and Mg′-value (0.47) and higher Fe_2O_3* content (13.1 wt.%) suggest that 564-17 is much more evolved than the other samples. Yet the greater CaO content (13.8 wt.%) and CaO/Al_2O_3 ratio (0.90) and much lower SiO_2 content (47 wt.%) of this basalt are characteristic of more primitive basalts (Basaltic Volcanism Study Project, 1981). The higher K_2O (0.62 versus 0.33 wt.%), Rb (15 versus 6 ppm), and Sr (115 versus 105 ppm), coupled with the other major element characteristics, may indicate that extreme seawater alteration has occurred.

In the plot of Ni versus Zr (Fig. 5), the Ni content decreases markedly with almost constant Zr in all Hole 564 samples, suggesting that olivine is the only liquidus phase. However, the Ni values (117 ppm) appear to be too high relative to the low CaO contents and CaO/Al_2O_3 ratios and high incompatible element abundances normally associated with a more evolved magma. As in the other holes, this discrepancy in the chemistry implies a complex petrogenesis.

There is a pronounced and systematic change in basalt composition with depth. MgO, Ni, and Cr abundances and Mg′-values all decrease downhole, whereas Fe_2O_3* and incompatible element (Nb, Zr, Y, and TiO_2) abundances increase (Appendix A, Table 7). The gradual changes of concentration with depth suggest that the earlier erupted magma was more evolved than the more recently erupted magma. Such changes are commensurate with the gradual emptying of a zoned magma chamber or the relatively rapid replenishment of a slowly evolving magma by more primitive melt.

The most striking aspect of chemical variation with depth is the change in Zr/Nb ratio, which is greater (>20) near the top of the hole, but gradually decreases downhole to <15 (Appendix A, Table 7; Fig. 8). However, this appears to be mostly the result of changing Nb. On the other hand, Zr/Y ratios remain essentially constant (2.8–3.0) with the downhole increase in Zr and Y (Fig. 7). Zr/Nb ratios are unlikely to change during crystal fractionation or more complex processes involving both fractionation and mixing of consanguineous magmas. Therefore, it seems probable that changes in the Zr/Nb ratio result from the progressive mixing of a primitive but Nb-enriched melt with one that was evolved but had lower Zr/Nb ratios.

Again, Sample 564-17 is different from the others; it has a lower Zr/Y ratio (2.7) and greater Y content (36 ppm) (Fig. 7). This inverse relationship is similar to that exhibited by Sample 559-1. There is no obvious explanation for this anomalous behavior, and further investigation is warranted. Two representative samples, one from the top and one from the bottom of Hole 564, will be analyzed for REE and isotopes.

DISCUSSION

Numerous isotopic and chemical studies have been made of basalts along the Mid-Atlantic Ridge from the Azores Triple Junction to south of the Hayes Fracture Zone (Fig. 1) (Schilling, 1975; White et al., 1976; O'Nions et al., 1977; Tarney et al., 1979; White and Schilling, 1978; Zindler et al., 1979; Dupré and Allègre, 1980; White and Hoffman, 1982). These studies have shown that the basalts from this area exhibit compositional diversity ranging from primitive to highly evolved and LREE-depleted to LREE-enriched (Types I and II of Bryan et al., 1976).

The holes sampled during Leg 82 (Fig. 1) contain several types of basalts that exhibit a variety of chemical characteristics and may occur together within a given hole (Table 1; Appendix A, Tables 1-7; Appendix B, Tables 1-7). Most of these chemical groups are uniform in composition, and, in general, simple crystal fractionation cannot be readily documented by chemical variation within groups. The exceptions are the olivine fractionation trend observed in Hole 558 (Group IV) (Figs. 2, 3, 5) and the plagioclase accumulation trends observed in Hole 562 (Group II) and Hole 563 (Figs. 2, 4).

Chemical variation, however, does exist between groups within a given hole. In Holes 556, 558, and 562 (Fig. 1), the decreasing CaO/Al_2O_3 ratios and increasing Zr/Y ratios (Figs. 4 and 7) seem to indicate that one group may have evolved from another by multiply saturated crystal fractionation. However, several lines of evidence indicate that the chemical variation between groups is not compatible with simple crystal fractionation. First, in these same three holes there is a discrepancy between estimates of the state of magmatic evolution based on major and compatible trace elements (e.g., MgO, CaO, Ni, Cr contents, Mg′-value, CaO/Al_2O_3 ratios) and that based on incompatible elements (TiO_2, Zr, Nb, Y) (Appendix A, Tables 2, 3, 5; Figs. 2–5). This discrepancy is clearly evident in Zr versus MgO and Ni (Figs. 2, 5), where associated groups in Holes 556, 558, and 562 have similar MgO and Ni abundances, but markedly different Zr contents. This phenomenon may imply that (1) each of the groups evolved from slightly different parental magmas or (2) the groups within each hole are related to a common parental magma by interplay of mixing and fractionation (Rhodes et al., 1979). The latter hypothesis receives further support from the existence

within Holes 556, 558, and 562 of different chemical groups with the same Sr but different Zr contents (Fig. 6). This cannot be explained by partial melting.

The stratigraphic interlayering of different chemical groups within the same hole (Holes 556 and 558) (Appendix A, Tables 1 and 2) indicates that similar magma compositions were episodically erupted. This supports the involvement of complex fractionation-mixing processes in the petrogenesis of these basalts. Further support comes from interlayered variations in Mg′-values in Holes 559 and 563 (Fig. 2), which could be due to repeated influxes of a more primitive melt into a more evolved magma (Rhodes et al., 1979). Further evidence for fractionation-mixing is the commonly observed discrepancy between the chemical criteria that appear to require clinopyroxene fractionation and the absence of clinopyroxene phenocrysts in any of the Leg 82 samples. This is a common problem in ocean-floor basalt petrogenesis (Dungan and Rhodes, 1978; Basaltic Volcanism Study Project, 1981) and is probably indicative of mixing between more-primitive and more fractionated magmas (Rhodes et al., 1979).

The systematic downhole trends in major and trace element abundances in Hole 564 (Appendix A, Table 7; Fig. 8) from relatively primitive to more evolved basalts is compatible with mixing of distinct magmas rather than simple crystal fractionation (Rhodes et al., 1979; Batiza and Johnson, 1980).

To gain a better understanding of Leg 82 basalt petrogenesis, it is important to assess the roles of mantle heterogeneity, complex melting, and melt segregation in the generation of the chemical diversity observed both within and between holes, especially Holes 558 and 561 (Table 1; Figs. 1–9; Appendix A, Tables 2, 4). For example, basalts with distinctly incompatible trace element ratios Zr/Y, Zr/Nb, and LREE/HREE (Figs. 7–9B) sampled within a single drill hole (Holes 558 and 561) have been cited as evidence for large-scale mantle heterogeneity involving a "depleted" upper mantle with mantle plumes upwelling from a more "fertile" deeper mantle layer (Schilling, 1973; Schilling et al., 1976; White and Schilling, 1978). Alternatively, mantle heterogeneity models involving mantle "blobs" (Schilling, 1975; Schilling et al., 1982), or pervasive small-scale veining or metasomatism of the upper mantle (Hanson, 1977; Zindler et al., 1979) have also been proposed. Complex melting and melt segregation in an otherwise homogeneous mantle (Langmuir et al., 1977; Wood, 1979) may cause similar differences in incompatible element and REE abundances, but not in ratios of highly incompatible elements $(La/Ce)_{ch}$ or Nd isotopes.

To evaluate these models it is necessary to develop a concept of the scale of heterogeneity with respect to both time and distance. The studies referenced above suggest the possibility of mantle "domains." For example, it appears that there is a boundary at about 33°N in the vicinity of the Hayes Fracture Zone separating depleted (Type I) MORBs (Bryan et al., 1976) to the south from enriched (Type II) basalts associated with the topographic high of the Azores Platform (White and Schilling, 1978; Bougault and Treuil, 1980).

In this study, basalts from holes drilled south of the Hayes Fracture Zone (Holes 562, 563, 564) (Fig. 1) are depleted in incompatible trace elements as expected. However, north of the Hayes Fracture Zone, basalts are both enriched (Holes 557 and 559) and depleted (Hole 556) in incompatible elements. At two sites (Holes 558 and 561), both types occur within the same hole (Figs. 1, 8, 9A, 9B). As other studies have shown (Blanchard et al., 1976; Langmuir et al., 1977; Tarney et al., 1979; Wood, 1979; Wood et al., 1979; Zindler et al., 1979), this close spatial association of enriched and depleted basalts is not uncommon. The occurrence of depleted basalts in older Hole 556 (30–34 Ma) and enriched basalts in younger Hole 557 (18 Ma) along a flow line from the Azores hot spot (Fig. 1) suggests that mantle anomalies are transient features, perhaps adding support to the mantle blob hypothesis (Schilling, 1975; Schilling et al., 1982) or small-scale mantle veining (Hanson, 1977; Zindler et al., 1979). In Hole 561, Groups I and II are not stratigraphically interlayered and have distinctly different ratios for the highly incompatible elements, Zr/Nb and $(La/Ce)_{ch}$, in addition to differences in Zr/Y, $(La/Sm)_{ch}$, and $(La/Yb)_{ch}$ ratios (Table 1; Figs. 7, 8, 9B). These traits suggest that Hole 561 basalts are derived from two distinct sources. Nd isotopic data (Jenner et al., this vol.) and geochemical data point to an LREE-enriched source for Group I and an LREE-depleted source for Group II (Table 1; Fig. 9B). The scale of the source heterogeneity cannot be pinpointed, although the presence within a single hole of magmas from two different sources may imply pervasive, small-scale heterogeneity such as mantle veining (Hanson, 1977; Zindler et al., 1979). The occurrence of only enriched basalts in older Hole 559 (34–37 Ma) along the same flow line as younger Hole 561 (14–17 Ma) (Fig. 1) could also be the result of a more transient mantle anomaly.

As noted above, variable incompatible and REE ratios within the same hole (such as Holes 558 and 561) may indicate either mantle heterogeneity or complex melting of a single source. If complex melting is involved, the ratios of the very highly incompatible elements, such as Zr/Nb and especially $(La/Ce)_{ch}$, should remain the same, whereas other ratios such as Zr/Y, $(La/Sm)_{ch}$, and $(La/Yb)_{ch}$ may vary (Langmuir et al., 1977; Wood, 1979). This is seen in Hole 558 where the $(La/Ce)_{ch}$ ratios are about the same (1.09–1.35) for all four groups (Table 1; Fig. 9A). In contrast, other incompatible and REE ratios vary from LREE enriched (Groups I, III, and IV) to LREE depleted (Group II) (Table 1; Figs. 7, 8, 9A; Appendix B, Table 2).

The data are not compatible with a petrogenesis involving only complex melting because Zr/Nb ratios vary considerably between Groups I, III, and IV (approximately 6–9) and Group II (20) (Fig. 8). Therefore, mantle heterogeneity may be indicated as well. The Nd isotopic ratios for Hole 558 basalts are almost identical for all four groups (Jenner et al., this vol.), so large-scale plume-related mantle heterogeneity involving two different sources does not seem likely.

A more plausible possibility is smaller-scale mantle veining and/or metasomatism (Hanson, 1977; Zindler

et al., 1979) that may generate the highly variable incompatible element ratios and crossing REE pattern observed in Hole 558, along with the constant $(La/Ce)_{ch}$ and Nd isotopic ratios. Similarly, the repetitive interlayering of diverse magmas within the same hole does not support large-scale mantle heterogeneity. Variation in trace element ratios and crossing REE patterns appear to be restricted to regions of high volcanic activity along elevated ridge segments in hot-spot areas. Other examples are the Juan de Fuca Ridge (Liias and Rhodes, 1982); Iceland (Wood, 1979; Zindler et al., 1979; Schilling et al., 1982); FAMOUS (Langmuir et al., 1977; White and Bryan, 1977); and Hole 558 (site chapter, Site 558, this vol.). The observation that such highly variable basalt types appear to be confined to hot-spot areas suggests small-scale heterogeneity as well as complex melting.

Basalts in Hole 556 have a drastically different chemical signature from the basalts in Hole 557 (Appendix A, Table 1) even though both holes were drilled on the same flow line through the Azores Triple Junction (Fig. 1). This chemical difference, along with the abrupt changes in the Zr/Nb ratios and REE patterns between chemical groups within Holes 558 and 561 (Figs. 8, 9A, 9B), is counter to the more gradual transitions expected between Type I and II basalts in plume or mantle blob situations (Schilling, 1975). The basalts from Leg 82 appear to have undergone a complex petrogenesis involving small-scale mantle heterogeneity (veining or metasomatism), complex melting, and mixing-fractionation processes.

CONCLUSIONS

1. There is no evidence for simple crystal fractionation within or between chemical groups, except for Hole 558 (Group IV), Hole 562 (Group II), and Hole 563 as discussed above.

2. The concept of widespread, complex fractionation-mixing processes is supported by several lines of evidence: (1) similar MgO, Ni, and Sr abundances with different amounts of incompatible elements in different chemical groups within the same hole; (2) episodic eruptions of similar magmas within the same hole; (3) stratigraphic interlayering of basalts with changing Mg′-values in Holes 559 and 563, suggesting that multiply saturated magmas were periodically replenished by more primitive melt; and (4) discrepancy between chemical composition requiring clinopyroxene fractionation and the lack of clinopyroxene phenocrysts in the samples, a widely observed problem in ocean-floor basalt petrogenesis.

3. The Hayes Fracture Zone appears to be a "domain" boundary between the depleted Type I basalts in the south and the highly variable basalts in the area between the Hayes Fracture Zone and the Azores Triple Junction (Fig. 1).

4. Hole 557 is one of the most highly enriched and/or evolved basalts sampled in the Atlantic Ocean (or anywhere else) (Melson et al., 1977; Basalt Volcanism Study Project, 1981). The composition of Sample 557-1 most closely resembles the FeTi basalts at the Galapagos Spreading Center (Schilling et al., 1976; Melson et al., 1977).

5. Although incompatible and REE ratios vary from depleted to enriched in Hole 558, $(La/Ce)_{ch}$ ratios (1.09–1.35) (Table 1; Fig. 9A) and Nd isotopic ratios (Jenner et al., this vol.) are nearly the same for all four groups in Hole 558. These constant ratios suggest that complex melting of a single source is probably the main process generating the observed compositional variations, although the varying Zr/Nb ratios (Fig. 8) may imply source variability on a small scale.

6. Variations in trace element ratios and crossing REE patterns appear to be restricted to the region of high volcanic activity along elevated ridge segments in a hot-spot area (in this case, the Azores Platform) (Fig. 1).

7. Two distinct sources are indicated for Hole 561 because the two (noninterlayered) chemical groups have distinctly different, highly incompatible element ratios, including $(La/Ce)_{ch}$ (Table 1; Fig. 9B) and $143_{Nd}/144_{Nd}$ (Jenner et al., this vol.).

8. The concept of more pervasive, small-scale mantle heterogeneity such as veining and/or metasomatism rather than a large-scale mantle plume or mantle blobs receives support from several lines of evidence: (1) restriction of high variability in trace element and REE ratios to hot-spot areas (Holes 556–561); (2) abrupt changes in Zr/Nb ratios (Fig. 8), REE patterns (Table 1; Figs. 9A and 9B), and Nd isotopic ratios (Jenner et al., this vol.) between different groups within the same hole (Holes 558 and 561); (3) drastic differences in composition and incompatible element ratios between the older, depleted basalts in Hole 556 (30–34 Ma) and the younger, highly enriched FeTi basalt in Hole 557 (18 Ma) (Appendix A, Table 1), which are about 22 Ma apart along the flow line passing through the Azores Triple Junction (Fig. 1); and (4) the existence of enriched basalts in older Hole 559 (34–37 Ma) and of both enriched and depleted basalts in younger Hole 561 (14–17 Ma) along the same flow line between the Oceanographer and Hayes fracture zones (Fig. 1).

9. The Azores hot-spot anomaly has existed in its present configuration for at least 18 Ma (Hole 557), but less than 30–34 Ma (Hole 556) (Fig. 1).

ACKNOWLEDGMENTS

We wish to thank the following people for their help in completing this study: F. Frey for use of the MIT INAA laboratory and P. Ila for sample preparation and instruction in using the lab; Marie Litterer for drafting the figures; Gerda Kunkel for typing the tables; and Karen Thatcher of Words-Worth for typing the manuscript and additional tables.

We also wish to express our appreciation to John F. Bender and John Longhi for their many helpful suggestions and meticulous care in reviewing this paper.

This research was funded by NSF Grant #7826330.

REFERENCES

Anderson, R. N., Clague, D. A., Klitgord, K. D., Marshall, M., and Nishimori, R. K,. 1975. Magnetic and petrologic variations along the Galapagos Spreading Center and their relation to the Galapagos melting anomaly. *Geol. Soc. Am. Bull.*, 86:683–694.

Basaltic Volcanism Study Project, 1981. *Basaltic Volcanism on the Terrestrial Planets:* New York (Pergamon Press), pp. 132–160.

Batiza, R., and Johnson, J. R., 1980. Trace element and isotopic evidence for magma mixing in alkalic and transitional basalts near the East Pacific Rise at 8°N. *In* Rosendahl, B.R., Hekinian, R., et

al., *Init. Repts. DSDP*, 54: Washington (U.S. Govt. Printing Office), 63–69.

Blanchard, D. P., Rhodes, J. M., Dungan, M. A., Rodgers, K. V., Donaldson, C. H., Brannon, J. C., Jacobs, J. W., and Gibson, E. K., 1976. Chemistry and petrology of basalts from Leg 37 of the Deep Sea Drilling Project. *J. Geophys. Res.*, 81:4231–4246.

Bougault, H., and Treuil, M., 1980. Mid-Atlantic Ridge: zero age geochemical variations between Azores and 22°N. *Nature*, 286: 209–212.

Bryan, W. B, Thompson, G., Frey, F. A., and Dickey, J. J., 1976. Inferred settings and differentiation in basalts from the Deep Sea Drilling Project. *J. Geophys. Res.*, 81:4285–4304.

Dungan, M. A., and Rhodes, J. M., 1978. Residual glasses and melt inclusions in basalts from DSDP Legs 45 and 46: evidence for magma mixing. *Contrib. Mineral. Petrol.*, 67:417–431.

Dupré, B., and Allègre, C. J,. 1980. Pb-Sr-Nd isotopic correlation and the chemistry of the North Atlantic mantle. *Nature*, 286:17–22.

Frey, F. A., Bryan, W. B., and Thompson, G., 1974. Atlantic Ocean floor: geochemistry and petrology of basalts from Legs 2 and 3 of the Deep Sea Drilling Project. *J. Geophys. Res.*, 79:5507–5527.

Hanson, G. N., 1977. Geochemical evolution of the sub-oceanic mantle. *J. Geol. Soc. London*, 134:235–253.

Jacobs, J. W., Korotev, R. L., Blanchard, D. P., and Haskin, L. A., 1977. A well-tested procedure for instrumental neutron activation analysis of silicate rocks and minerals. *J. Radioanal. Chem.*, 40: 93–114.

Langmuir, C. H., Bender, J. F., Bence, A. E., Hanson, G. N., and Taylor, S. R., 1977. Petrogenesis of basalts from the FAMOUS area: Mid-Atlantic Ridge. *Earth Plant. Sci. Lett.*, 36:133–156.

Liias, R. A., and Rhodes, J. M., 1982. Does a mantle plume influence basalt composition along the Juan de Fuca Ridge? *EOS, Trans. Am. Geophys. Union*, 63:1153–1154. (Abstract)

Melson, W. G., Byerly, G. R., Nelen, J. A., O'Hearn, T., Wright, T. L., and Vallier, T. L., 1977. A catalog of the major element chemistry of abyssal volcanic glasses. *Smithson. Contrib. Earth Sci.*, 19:31–60.

Melson, W. G., and O'Hearn, T., 1979. Basaltic glass erupted along the Mid-Atlantic Ridge between 0–37°N; relationships between composition and latitude. *In* Talwani, M., Harrison, C. G., and Hayes, D. E. (Eds.), *Deep Drilling Results in the Atlantic Ocean: Ocean Crust:* Washington (Am. Geophys. Union), pp. 249–261.

Norrish, K., and Chappell, B. W., 1967. X-ray fluorescence spectrometry. *In* Zussman, J. (Ed.), *Physical Methods in Determinative Mineralogy:* New York (Academic Press), pp. 161–214.

Norrish, K., and Hutton, J. T., 1969. An accurate X-ray spectrographic method for the analysis of a wide range of geological samples. *Geochim. Cosmochim. Acta*, 33:431–453.

O'Nions, R. K., Hamilton, P. J., and Evensen, N. M., 1977. Variation in $^{143}Nd/^{144}Nd$ and $^{87}Sr/^{86}Sr$ ratios in oceanic basalts. *Earth Planet Sci. Lett.*, 34:13–22.

Reynolds, R. C., 1967. Matrix corrections in trace element analysis by X-ray fluorescence: estimation of the mass absorption coefficient by Compton scattering. *Am. Mineral.*, 48:1133–1143.

Rhodes, J. M., Dungan, M. A., Blanchard, D. P., and Long, P. E., 1979. Magma mixing at mid-ocean ridges: evidence from basalts drilled near 22°N on the Mid-Atlantic ridge. *Tectonophysics*, 55: 36–61.

Schilling, J.-G., 1973. Iceland mantle plume: geochemical study of Reykjanes Ridge. *Nature*, 242:565–575.

_____, 1975. Azores mantle blob: Rare earth evidence. *Earth Planet. Sci. Lett.*, 25:103–115.

Schilling, J.-G., Anderson, R. N., and Vogt, P., 1976. Rare earth, Fe, and Ti variations along the Galapagos spreading centre, and their relationship to the Galapagos mantle plume. *Nature*, 261:108–113.

Schilling, J.-G., Meyer, P. S., and Kingsley, R. H., 1982. Evolution of the Iceland hot spot. *Nature*, 296:313–320.

Tarney, J., Wood, D. A., Varet, J., Saunders, A. D., and Cann, J. R., 1979. Nature of mantle heterogeneity in the North Atlantic: evidence from Leg 49 basalts. *Proc. Second M. Ewing Symp.*, pp. 285–301.

White, W. M., and Bryan, W. B., 1977. Sr-isotope, K, Rb, Cs, Sr, Ba and rare-earth geochemistry of basalts from the FAMOUS area. *Geol. Soc. Am. Bull.*, 88:571–576.

White, W. M., and Hofmann, A. W., 1982. Sr and Nd isotope geochemistry of oceanic basalts and mantle evolution. *Nature*, 296: 821–825.

White, W. M., and Schilling, J.-G., 1978. The nature and origin of geochemical variation in Mid-Atlantic Ridge basalts from central North Atlantic. *Geochim. Cosmochim. Acta*, 42:1501–1516.

White, W. M., Schilling, J.-G., and Hart, S. R., 1976. Evidence for the Azores mantle plume from strontium isotope geochemistry of the central North Atlantic. *Nature*, 263:659–663.

Wood, D. A., 1979. Dynamic partial melting: its application to the petrogenesis of basalts erupted in Iceland, the Faeroe Islands, the Isle of Skye (Scotland) and the Troodos Massif (Cypress). *Geochim. Cosmochim. Acta*, 43:1031–1046.

Wood, D. A., Tarney, J., Varet, J., Saunders, A. A., Bougault, H., Joron, J. L., Treuil, M., and Cann, J., 1979. Geochemistry of basalts drilled in the North Atlantic by IPOD Leg 49: implications for mantle heterogeneity. *Earth Planet. Sci. Lett.*, 42:77–97.

Zindler, A., Hart, S. R., Frey, F. A., and Jakobsson, S. P., 1979. Nd and Sr isotope ratios and rare earth element abundances in Reykjanes Peninsula basalts: evidence for mantle heterogeneity beneath Iceland. *Earth Planet. Sci. Lett.*, 45:249–262.

Date of Initial Receipt: 18 November 1983
Date of Acceptance: 4 April 1984

APPENDIX A
Chemical Compositions of Basalts from Leg 82

Note to Appendix A tables: Chemical group refers to chemical groups discussed in text. Fe_2O_3* and FeO^+ refer to total Fe expressed as Fe^{3+} and Fe^{2+}, respectively. Calculation of Mg′-value discussed in text (Mg/[Mg + Fe^2]). Small discrepancies in totals may be attributed to rounding.

Table 1. Holes 556 and 557.

Univ. Mass. sample no.	556-1 Hole 556	556-2 Hole 556	556-3 Hole 556	556-4 Hole 556	556-5 Hole 556	556-6 Hole 556	556-7 Hole 556	556-8 Hole 556	556-9 Hole 556	556-10 Hole 556	556-11 Hole 556	556-12 Hole 556	556-13 Hole 556	556-14 Hole 556	556-15 Hole 556	556-16 Hole 556	556-17 Hole 556	557-1 Hole 557
Core-Section	2-1	2-2	2-5	3-3	5-1	6-5	6-6	7-1	7-3	8-2	9-4	10-3	10-4	11-2	12-3	12-4	16-2	1-1
(interval in cm)	74–76	141–144	26–28	66–69	99–102	64–67	108–111	128–132	83–86	13–16	64–67	63–66	72–75	121–124	54–57	27–30	110–113	50–53
Sub-bottom depth (m)	462.25	464.43	467.77	474.77	490.01	504.66	506.60	508.30	510.85	517.65	530.16	537.65	539.24	545.73	555.56	556.78	586.1	461.02
Chemical group	IA	IA	II	II	II	II	IA	IA	IA	IB	IA	IB	IA	IA	IA	IA	IB	II
Major elements (wt.%)																		
SiO_2	50.55	50.22	50.04	50.03	50.21	50.69	49.50	50.12	50.02	50.37	50.85	49.71	50.26	50.41	50.33	50.46	50.10	47.87
TiO_2	1.05	1.05	1.49	1.41	1.49	1.39	1.00	1.03	1.03	0.88	1.08	0.83	0.99	1.02	0.97	0.99	0.88	3.67
Al_2O_3	15.63	15.96	16.05	15.46	15.97	16.33	16.28	15.89	16.11	15.85	15.38	17.79	16.38	15.49	16.28	16.00	15.64	12.73
Fe_2O_3*	9.54	8.72	10.91	11.42	10.83	9.75	8.43	10.08	8.98	8.33	9.49	7.55	8.72	9.19	8.91	9.11	8.59	16.51
MnO	0.15	0.15	0.17	0.18	0.17	0.17	0.15	0.16	0.17	0.14	0.15	0.12	0.15	0.16	0.14	0.15	0.16	0.22
MgO	7.58	7.51	6.64	6.92	6.58	6.84	7.59	7.17	7.33	7.87	7.60	7.19	7.09	7.57	7.58	7.26	7.54	5.01
CaO	12.52	13.31	11.72	11.74	11.57	11.80	14.39	12.74	13.36	14.25	12.57	14.16	13.53	13.38	12.90	12.88	14.27	10.00
Na_2O	2.01	2.02	2.83	2.58	2.46	3.09	2.59	2.60	2.51	2.38	2.76	2.54	2.33	2.26	2.21	2.30	2.09	2.66
K_2O	0.35	0.20	0.31	0.37	0.27	0.14	0.24	0.29	0.35	0.27	0.33	0.25	0.38	0.38	0.33	0.53	0.24	0.52
P_2O_5	0.12	0.12	0.15	0.16	0.16	0.14	0.11	0.11	0.11	0.11	0.11	0.10	0.12	0.10	0.11	0.11	0.11	0.41
Total	99.50	99.28	100.31	100.27	99.71	100.34	100.26	100.20	99.98	100.44	100.32	100.24	99.94	99.96	99.75	99.78	99.61	99.59
Trace elements (ppm)																		
Rb	7.1	2.4	5.5	7.1	4.3	1.8	2.3	6.3	4.1	3.2	10.7	3.8	10.7	9.4	5.7	14.4	2.8	10.8
Sr	105	104	101	99	101	98	101	99	97	99	99.3	99.1	97.2	103.6	95.7	94.1	98.5	299.0
Y	23.4	23.9	32.7	30.7	33.1	30.7	22.6	22.2	23.3	20.4	24.3	18.2	21.5	23.0	21.8	21.3	20.1	41.0
Ga	15.7	15.2	16.7	16.1	16.4	17.0	14.7	15.4	15.0	14.0	15.2	16.1	15.4	15.5	14.7	15.0	14.3	22.6
Zr	62	64	97	89	87	88	56	58	56	48	60.4	46.4	58.1	56.0	55.6	58.2	50.4	216.2
Nb	2.3	2.3	2.2	2.4	2.6	2.7	2.2	1.2	2.0	2.1	1.9	2.4	1.7	1.2	1.0	1.5	1.6	26.2
Zn	77	75	92	84	87	97	73	68	74	68	80.1	76.1	77.3	69.0	71.0	65.4	69.4	113.3
Ni	95	178	84	88	88	97	145	91	81	106	73.3	90.0	90.2	73.0	91.6	91.2	135.7	38.3
Cr	311	277	235	251	251	280	366	331	373	284	93.8	381.2	404.6	239.6	387.7	395.4	291.6	18.7
V	241	238	55	238	238	250	215	208	218	221	253.2	201.9	229.4	228.0	222.9	224.7	231.5	300.0
Mg′-value	0.64	0.65	0.57	0.57	0.57	0.61	0.66	0.61	0.64	0.68	0.64	0.68	0.64	0.64	0.65	0.64	0.66	0.40
FeO*	8.58	7.85	9.82	10.28	9.75	8.77	7.59	9.07	8.08	7.50	8.54	6.79	7.85	8.27	8.02	8.20	7.73	14.86
CaO/Al_2O_3	0.80	0.83	0.73	0.76	0.72	0.72	0.88	0.80	0.83	0.90	0.82	0.80	0.83	0.86	0.79	0.81	0.91	0.61
Zr/Nb	27.2	27.7	43.9	37.0	37.5	32.6	25.5	48.4	28.2	23.1	31.8	19.3	34.2	46.7	55.6	38.8	31.5	8.3
Zr/Y	2.67	2.67	2.96	2.89	2.95	2.86	2.49	2.62	2.42	2.38	2.49	2.55	2.70	2.43	2.55	2.73	2.51	5.27

Note: See note at beginning of Appendix A.

Table 2. Hole 558.

Univ. Mass. sample no.	558-1	558-2	558-3	558-4	558-5	558-6	558-7	558-8	558-9	558-10	558-11	558-12	558-13	558-14	558-15	558-16
Core-Section	27-3	28-1	30-1	32-2	32-4	32-5	33-2	33-3	33-3	35-3	36-1	37-1	38-1	38-2	39-1	39-2
(interval in cm)	112–114	55–58	115–118	130–132	73–75	101–103	144–147	61–64	139–141	107–109	74–78	89–92	97–99	116–118	111–113	11–13
Sub-bottom depth (m)	409.13	415.07	433.67	453.31	455.74	457.51	462.46	463.13	463.90	481.58	487.26	496.41	505.48	507.17	510.12	510.62
Chemical group	IA	II	IIIA	IIIB	IIIB	IIIB	IIIB	IIIB	IIIB	IA	IB	IV	IV	IV	IV	IV
Major elements (wt.%)																
SiO_2	50.60	51.09	50.32	50.33	50.42	49.94	50.38	50.29	49.93	49.43	49.22	49.35	49.12	49.45	48.89	49.61
TiO_2	1.25	1.16	1.45	1.35	1.30	1.30	1.31	1.30	1.31	1.22	1.31	0.98	0.95	0.99	1.02	0.96
Al_2O_3	14.64	15.82	15.16	15.40	14.86	15.30	14.85	14.92	15.34	15.03	15.54	16.15	15.70	16.15	16.61	15.60
Fe_2O_3*	10.32	8.80	10.46	9.36	9.83	9.91	9.83	9.86	9.72	10.14	10.43	9.90	9.87	10.10	10.48	9.87
MnO	0.15	0.16	0.15	0.14	0.17	0.14	0.17	0.16	0.15	0.17	0.18	0.14	0.17	0.16	0.17	0.18
MgO	9.53	8.26	8.17	8.67	8.97	8.78	9.01	9.05	8.70	8.92	7.82	8.33	10.80	8.33	7.54	9.89
CaO	10.62	12.40	11.58	11.89	11.63	11.70	11.55	11.51	11.74	12.13	12.26	12.04	11.71	12.21	12.92	11.71
Na_2O	2.21	2.15	2.30	2.24	2.13	2.35	1.84	1.88	2.36	2.52	2.28	2.16	2.09	2.12	2.32	2.17
K_2O	0.26	0.17	0.46	0.40	0.31	0.41	0.30	0.30	0.38	0.35	0.41	0.29	0.22	0.23	0.30	0.29
P_2O_5	0.15	0.12	0.21	0.19	0.17	0.19	0.18	0.18	0.18	0.16	0.20	0.14	0.13	0.13	0.14	0.13
Total	99.72	100.14	100.27	99.97	99.80	100.04	99.40	99.45	99.81	100.06	99.63	99.48	100.76	99.87	100.38	100.40
Trace elements (ppm)																
Rb	3.6	2.5	9.7	2.5	6.6	6.8	5.4	6.8	6.9	6	7.7	7	3.7	3.9	4.9	5
Sr	128.9	94.7	170	179.5	174.8	176.4	174.5	173	175.2	142.2	145.9	111.2	108.2	114.1	116.2	109.1
Y	22.2	25.6	24.2	21.8	21.6	21.2	21.8	21.1	21.2	22.5	24	18.5	18.5	19.2	19.2	18.2
Ga	15.7	16	15.6	15.1	15.4	14	15.4	14.8	16.2	14.8	15.3	14.7	15.2	14.3	15.4	14.3
Zr	75.87	66.53	92.80	84.62	82.60	81.50	82.19	82.79	80.24	75.99	85.64	55.40	54.76	57.29	57.86	55.74
Nb	8.64	3.10	15.25	13.75	14.49	13.39	13.41	13.98	12.65	9.53	11.34	7.57	7.24	7.75	7.74	7.44
Zn	83	90.33	89.45	85.61	83.87	81.33	87.74	98.53	84.74	87.02	87.44	78.63	73.14	82.6	88.65	72.26
Ni	277.4	169.8	157.5	170.6	156.2	157.9	156.1	155.9	175.0	185.8	152.5	208.3	230.1	219.6	184.88	213.6
Cr	509.7	400.5	356.3	367.0	388.9	371.6	384.8	398.3	362.8	380.5	308.5	458.4	449.4	481.5	476.6	441.5
V	195.6	238.3	257.9	242.8	249.8	233.9	243.7	252.0	233.4	239.9	246.4	197.6	190.5	211.5	224.4	191.6
Mg'-value	0.67	0.67	0.63	0.67	0.67	0.66	0.67	0.67	0.66	0.66	0.62	0.65	0.71	0.65	0.62	0.69
FeO*	9.29	7.92	9.41	8.42	8.85	8.92	8.85	8.87	8.75	9.12	9.39	8.90	8.88	9.09	9.43	8.88
CaO/Al_2O_3	0.73	0.78	0.76	0.77	0.78	0.76	0.78	0.77	0.77	0.81	0.79	0.75	0.75	0.76	0.78	0.75
Zr/Nb	8.78	21.46	6.09	6.15	5.70	6.09	6.13	5.92	6.34	7.97	7.55	7.32	7.56	7.39	7.48	7.49
Zr/Y	3.42	2.60	3.83	3.88	3.82	3.84	3.77	3.92	3.78	3.38	3.57	2.99	2.96	2.98	3.01	3.06

Note: See note at beginning of Appendix A.

Table 3. Hole 559.

Univ. Mass. sample no.	559-1	559-2	559-3	559-4	559-5	559-6	559-7	559-8	559-9
Core-Section	1-1	2-3	4-1	5-1	6-2	7-1	7-3	7-3	8-3
(interval in cm)	117–119	111–113	121–124	50–53	14–16	111–114	18–20	103–106	6–10
Sub-bottom depth (m)	239-18	251.12	257.72	265.51	275.65	284.12	286.19	287.19	295.08
Major elements (wt.%)									
SiO_2	49.23	50.62	49.90	49.50	49.67	48.48	49.68	49.97	48.65
TiO_2	1.61	1.52	1.54	1.54	1.54	1.59	1.54	1.52	1.50
Al_2O_3	16.19	15.49	15.35	15.40	15.39	15.86	15.31	14.97	15.14
Fe_2O_3*	11.30	9.93	10.44	11.21	10.59	11.71	10.77	10.80	12.02
MnO	0.17	0.12	0.16	0.19	0.15	0.19	0.15	0.16	0.24
MgO	6.45	7.84	7.56	6.69	7.28	6.38	7.46	7.52	6.77
CaO	11.73	11.57	11.78	11.94	11.69	12.35	11.35	11.24	11.98
Na_2O	2.76	2.70	2.64	2.77	2.39	2.47	2.54	2.59	2.33
K_2O	0.62	0.35	0.38	0.44	0.44	0.42	0.51	0.39	0.69
P_2O_5	0.25	0.20	0.21	0.21	0.20	0.24	0.20	0.21	0.20
Total	100.30	100.34	99.96	99.89	99.35	99.69	99.51	99.38	99.52
Trace elements (ppm)									
Rb	9.9	5.9	5.2	6.5	7.4	6.9	7.0	7.0	17.0
Sr	167.9	162.5	162.8	166.6	161.8	171.4	161.8	161.1	169.0
Y	31.6	27.1	28.3	28.0	27.8	29.2	28.2	27.6	27.1
Ga	13.3	15.7	15.8	16.0	17.2	16.9	16.5	15.7	17.2
Zr	108.4	105.4	107.0	105.7	107.5	111.6	106.8	107.0	103.1
Nb	15.5	14.4	15.0	15.2	14.7	15.6	15.4	15.0	14.5
Zn	176.0	90.4	98.3	102.7	91.0	96.6	96.5	88.3	83.6
Ni	103.9	211.2	142.0	126.9	127.3	113.2	121.0	108.9	134.4
Cr	163.8	254.7	267.3	260.9	277.1	276.1	247.3	245.5	253.6
V	291.9	246.5	266.8	276.9	267.1	291.9	253.8	252.7	253.6
Mg'-value	0.56	0.63	0.61	0.57	0.60	0.55	0.60	0.61	0.55
FeO*	10.17	8.94	9.39	10.09	9.53	10.54	9.69	9.72	10.82
CaO/Al_2O_3	0.72	0.75	0.77	0.78	0.76	0.78	0.74	0.75	0.79
Zr/Nb	6.99	7.32	7.13	6.95	7.31	7.15	6.94	7.13	7.11
Zr/Y	3.43	3.89	3.78	3.78	3.87	3.82	3.79	3.88	3.80

Note: See note at beginning of Appendix A. All samples belong to Chemical Group I.

Table 4. Hole 561.

Univ. Mass. sample no.	561-1	561-2	561-3	561-4	561-5	561-6	561-7	561-8	561-9
Core-Section	HI-CC	1-1	1-1	1-2	2-1	2-2	3-1	3-1	3-2
(interval in cm)	3–5	4–9	84–87	24–26	100–103	82–84	9–13	76–79	77–80
Sub-bottom depth (m)	8.60	411.57	412.36	413.25	415.52	416.83	417.61	424.28	425.79
Chemical group	I	I	II	II	II	II	II	II	II
Major elements (wt.%)									
SiO_2	49.71	49.75	50.45	50.13	50.25	49.99	50.11	50.09	50.05
TiO_2	1.23	1.21	1.37	1.35	1.33	1.35	1.34	1.39	1.37
Al_2O_3	15.49	15.26	15.29	15.05	14.96	15.28	14.88	15.10	14.79
Fe_2O_3*	9.97	9.87	11.08	11.61	11.82	10.94	1.89	11.39	11.41
MnO	0.16	0.15	0.18	0.18	0.18	0.20	0.18	0.17	0.18
MgO	7.93	8.18	7.34	7.48	7.08	7.85	7.22	7.44	7.67
CaO	12.33	12.10	11.66	11.31	11.42	11.66	11.49	11.69	11.83
Na_2O	2.48	2.51	2.72	2.57	2.58	2.55	2.59	2.53	2.24
K_2O	0.37	0.36	0.34	0.30	054	0.28	0.50	0.29	0.26
P_2O_5	0.23	0.23	0.13	0.14	0.13	0.13	0.13	0.13	0.13
Total	99.89	99.62	100.47	100.12	100.28	100.23	100.33	100.22	99.91
Trace elements (ppm)									
Rb	5.4	5.5	6.8	6.9	13.8	6.5	12.1	6.6	5.2
Sr	216	215	100	88	87	90	86	86	85
Y	25.5	25.5	32.3	31.4	30.7	31.7	31.0	32.6	32.4
Ga	15.6	14.8	18.1	17.6	17.4	17.4	16.8	17.0	17.7
Zr	102	100	76	75	71	73	73	77	76
Nb	21.9	21.6	3.5	2.1	2.6	2.6	3.1	2.0	3.0
Zn	85	93	104	109	96	106	96	101	101
Ni	166	186	120	123	126	159	114	128	138
Cr	416	413	228	245	222	237	217	236	238
V	240	236	297	305	292	302	290	313	311
Mg′-value	0.62	0.65	0.59	0.59	0.57	0.61	0.57	0.59	0.60
FeO*	0.97	8.88	9.97	10.45	10.64	9.84	10.70	10.25	10.27
CaO/Al_2O_3	0.80	0.79	0.77	0.75	0.76	0.76	0.77	0.77	0.80
Zr/Nb	4.7	4.6	21.8	35.2	26.9	28.0	23.7	38.6	25.2
Zr/Y	3.99	3.92	2.34	2.38	2.31	2.32	2.36	2.37	2.33

Note: See note at beginning of Appendix A.

Table 5. Hole 562.

Univ. Mass. sample no.	562-1	562-2	562-3	562-4	562-5	562-6	562-7	562-8	562-9	562-10	562-11	562-12	562-13	562-14	562-15	562-16
Core-Section	H1-CC	2-3	4-1	5-1	5-4	6-3	6-4	7-2	8-1	8-1	8-2	9-1	9-1	10-1	10-3	11-1
(interval in cm)	16–19	8–10	75–77	64–66	29–31	135–138	6–10	56–58	132–134	144–146	25–29	82–84	145–147	90–93	52–55	115–117
Sub-bottom depth (m)	243.23	253.09	268.76	277.65	281.80	290.37	290.58	297.07	301.33	301.45	306.77	304.77	305.46	313.92	316.54	323.16
Chemical group	I	I	I	I	I	I	I	I	I	I	II	II	II	II	II	II
Major elements (wt.%)																
SiO_2	49.23	49.91	49.83	50.32	49.52	49.32	50.19	49.98	49.67	49.43	48.90	48.33	49.78	49.12	49.72	49.18
TiO_2	1.57	1.58	1.60	1.58	1.54	1.54	1.20	1.20	1.25	1.30	1.16	1.19	1.28	1.26	1.29	1.15
Al_2O_3	15.71	15.31	15.21	15.97	15.82	15.69	17.27	16.22	16.38	15.50	17.11	16.73	15.75	16.01	15.38	17.43
Fe_2O_3*	11.90	11.79	11.75	10.70	11.25	11.54	8.95	10.34	9.89	10.17	9.91	9.89	10.57	11.07	10.60	9.81
MnO	0.18	0.18	0.19	0.16	0.17	0.20	0.13	0.16	0.16	0.17	0.15	0.18	0.17	0.18	0.17	0.16
MgO	6.71	7.24	7.41	6.73	7.05	7.03	6.94	7.19	7.28	7.61	7.37	7.28	7.16	7.09	7.82	6.52
CaO	11.64	11.53	11.42	11.85	11.53	11.84	12.90	12.31	12.63	13.23	12.97	13.85	12.44	12.96	12.45	12.92
Na_2O	2.29	2.42	2.55	2.52	2.70	2.63	2.14	2.01	2.17	2.20	1.97	2.04	2.04	2.1	2.02	1.91
K_2O	0.25	0.31	0.13	0.21	0.10	0.35	0.18	0.22	0.21	0.25	0.21	0.22	0.38	0.32	0.26	0.25
P_2O_5	0.15	0.14	0.17	0.16	0.15	0.16	0.13	0.12	0.13	0.13	0.13	0.13	0.14	0.14	0.13	0.12
Total	99.63	100.41	100.26	100.19	99.83	100.30	100.02	99.75	99.79	99.98	99.88	99.84	99.69	100.24	99.84	99.46
Trace elements (ppm)																
Rb	2.6	5.6	1.9	2.3	1.2	6.7	3.1	3.5	3.9	4.5	3.3	4.1	8.2	6.1	4.6	4.7
Sr	105	96.6	94.4	99.5	102.1	103.6	91.9	97.5	96.4	108.4	90.4	101.3	114.4	95.1	89.6	94.5
Y	36.1	35.1	35	34.9	34.4	32.9	26.5	26.3	27.7	29.4	25.1	26	28.7	28	28.5	25.2
Ga	17.5	17.3	17.8	17.3	17.1	17.9	16.1	16.3	16.5	16.1	15.5	16.1	16.9	16.6	16.5	15.9
Zr	96.5	97.3	92.4	96.4	93.4	93	69	67.5	72.1	74.3	65.7	67.8	73.4	73.3	74	65
Nb	3.1	3.9	3.8	3.4	3.2	3.1	2.5	2.2	2.7	2.5	2.3	3.0	2.3	2.7	2.5	2.8
Zn	103.9	95.6	90.1	95.8	86.6	106.2	83	80.1	88.1	93.1	81.2	83.6	93.9	99.3	95.2	81.1
Ni	109.2	107.6	106	119.5	105.1	109.2	169.5	105.7	102	121.6	98.7	109.6	112.5	104.2	124.4	98.2
Cr	241.8	236.5	211.1	235.4	215.3	246.6	244.9	242.8	262	267.8	248.6	251.2	265.1	264.2	268.1	250.6
V	313.8	298.9	284.1	286.7	274	286.1	250	243.3	267	278.4	243.4	254.6	282.7	277.3	279.9	244.2
Mg′-value	0.55	0.57	0.58	0.58	0.58	0.57	0.63	0.60	0.62	0.62	0.62	0.62	0.60	0.58	0.62	0.59
FeO*	10.71	10.61	10.57	9.63	10.12	10.38	8.05	9.30	8.90	9.15	8.92	8.90	9.51	9.96	9.54	8.83
CaO/Al_2O_3	0.74	0.75	0.75	0.74	0.73	0.75	0.75	0.76	0.77	0.85	0.76	0.83	0.79	0.81	0.81	0.74
Zr/Nb	31.1	24.9	25.6	28.4	29.2	30.0	27.6	30.7	26.7	29.7	28.6	22.6	31.9	27.1	29.6	23.2
Zr/Y	2.67	2.77	2.78	2.76	2.72	2.83	2.60	2.55	2.60	2.53	2.62	2.61	2.56	2.62	2.60	2.58

Note: See note at beginning of Appendix A.

Table 6. Hole 563.

Univ. Mass sample no.	563-1	563-2	563-3	563-4	563-5	563-6	563-7	563-8
Core-Section	23-1	24-1	24-1	24-2	24-2	24-4	25-1	25-2
(interval in cm)	115–117	22–25	57–60	93–95	123–127	7–10	36–38	115–117
Sub-bottom depth (m)	365.66	366.74	367.09	368.94	369.94	371.09	373.87	376.16
Major elements (wt.%)								
SiO_2	49.73	49.47	49.76	49.23	49.98	49.58	49.79	49.96
TiO_2	1.02	0.97	1.05	0.97	1.05	0.99	0.98	1.01
Al_2O_3	15.78	16.40	15.26	16.09	15.40	16.02	16.37	15.85
Fe_2O_3	10.18	10.26	9.98	10.43	9.89	10.07	9.72	10.35
MnO	0.17	0.15	0.15	0.17	0.16	0.17	0.16	0.17
MgO	7.61	7.47	8.04	7.54	8.03	7.35	7.80	7.55
CaO	13.20	13.07	12.94	13.00	13.01	13.41	12.97	13.06
Na_2O	1.96	1.88	1.97	2.29	2.21	1.93	2.20	2.20
K_2O	0.26	0.32	0.26	0.29	0.25	0.31	0.20	0.27
P_2O_5	0.09	0.10	0.10	0.09	0.09	0.10	0.09	0.11
Total	99.99	100.11	99.52	100.09	100.06	99.93	100.27	100.53
Trace elements (ppm)								
Rb	5.5	7.4	5.2	6.8	5	6.8	2.5	5.7
Sr	86.7	83.3	86	82.1	82.5	82.3	82.6	83.7
Y	23.7	22.8	24.9	22.8	25.1	22.9	21.6	23.6
Ga	15.1	15.9	15.6	15.7	15.4	14.9	15.4	15.5
Zr	55.9	52.5	59.2	55.3	60.02	54.7	54.5	54.9
Nb	2.6	2.11	2.9	1.7	2.6	2.5	2.2	2.6
Zn	81.3	78.0	81.1	78.0	96.2	78.9	77.8	79.1
Ni	110.3	97.97	95.3	103.8	106.9	106.8	106.9	96.7
Cr	330.2	322.8	338.1	326.1	350.9	318.7	322.6	324.9
V	293.4	279.8	306.4	285.5	310.7	286.1	272.9	298.0
Mg′-value	0.63	0.62	0.64	0.61	0.64	0.62	0.64	0.62
FeO*	9.16	9.20	8.98	9.39	8.90	9.06	8.75	9.51
CaO/Al_2O_3	0.84	0.80	0.85	0.81	0.84	0.84	0.79	0.82
Zr/Nb	27.95	24.89	20.41	32.53	23.15	21.88	24.77	21.12
Zr/Y	2.36	2.30	2.38	2.43	2.40	2.39	2.52	2.33

Note: See note at beginning of Appendix A. All samples belong to Chemical Group I.

Table 7. Hole 564.

Univ Mass. sample no.	564-1	564-2	564-3	564-4	564-5	564-6	564-7	564-8	564-9	564-10	564-11	564-12	564-13	564-14	564-15	564-16	564-17	564-18	564-19	564-20
Core-Section	H1-CC	1-1	1-3	2-2	2-3	3-2	4-2	4-4	5-2	5-4	6-1	6-4	6-5	7-1	7-3	8-2	9-1	9-1	9-2	9-3
(interval in cm)	11–15	129–131	38–40	3–5	18–20	35–37	37–41	140–142	89–91	24–27	15–18	48–52	32–34	12–15	13–15	7–10	18–20	140–143	128–130	68–71
Sub-bottom depth (m)	282.61	285.30	287.39	294.54	296.19	303.86	312.89	316.91	322.40	324.76	329.17	334.00	335.33	338.14	341.14	348.59	356.19	357.42	358.79	359.70
Major elements (wt.%)																				
SiO_2	49.35	50.21	49.86	49.57	50.58	49.62	49.87	49.88	50.39	49.44	50.54	49.42	50.17	49.77	50.63	49.87	47.24	49.11	48.99	49.34
TiO_2	1.48	1.43	1.40	1.44	1.47	1.45	1.46	1.45	1.46	1.51	1.48	1.44	1.50	1.49	1.52	1.48	1.52	1.53	1.58	1.55
Al_2O_3	15.77	14.94	14.71	15.22	15.17	14.92	14.89	14.76	14.69	14.99	14.64	14.38	14.64	14.5	14.73	14.56	15.16	15.08	15.04	14.96
Fe_2O_3*	11.55	11.29	11.58	11.60	10.11	11.71	11.92	11.82	11.82	12.37	11.86	12.31	11.95	11.96	11.56	11.90	13.07	12.01	12.53	12.56
MnO	0.19	0.18	0.17	0.18	0.17	0.20	0.20	0.16	0.17	0.19	0.17	0.19	0.18	0.17	0.18	0.17	0.19	0.18	0.18	0.20
MgO	6.13	7.52	7.59	7.00	7.77	7.32	7.32	7.54	7.48	6.78	7.24	8.43	7.48	7.42	6.99	7.54	5.20	6.86	6.70	6.81
CaO	12.82	11.89	11.63	12.15	12.05	11.92	11.76	11.52	11.52	11.76	11.42	11.28	11.53	11.45	11.67	11.40	13.83	11.76	11.86	11.87
Na_2O	2.51	2.47	2.76	2.39	2.26	2.82	2.31	2.56	2.48	2.58	2.12	2.05	2.08	2.10	2.15	2.22	2.26	2.66	2.28	2.44
K_2O	0.44	0.35	0.36	0.39	0.20	0.38	0.36	0.36	0.19	0.40	0.19	0.24	0.33	0.41	0.23	0.42	0.62	0.36	0.35	0.33
P_2O_5	0.16	0.14	0.15	0.16	0.15	0.14	0.15	0.17	0.16	0.17	0.16	0.16	0.17	0.16	0.16	0.16	0.21	0.17	0.17	0.17
Total	100.40	100.42	100.22	100.10	99.93	100.47	100.26	100.22	100.34	100.19	99.83	99.92	100.03	99.42	99.82	99.73	99.31	99.73	99.67	100.23
Trace elements (ppm)																				
Rb	7.5	6.4	6.0	5.8	2.7	6.3	5.8	7.2	2.6	7.0	2.3	4.9	5.7	7.2	2.6	7.5	14.7	6.9	6.2	6.3
Sr	115.1	106.8	101.8	103.6	108.1	105.5	103.0	99.9	99.5	105.6	100.9	104.8	101.2	103.6	102.1	103.2	114.6	106.9	107.9	107.2
Y	31.7	32.2	31.8	32.3	33.7	32.8	32.5	32.2	32.7	33.6	33.4	31.9	33.0	33.3	34.2	32.5	35.6	33.4	34.1	33.8
Ga	17.4	16.1	16.4	17.2	18.0	17.2	16.6	16.4	17.2	17.2	16.6	16.4	17.0	17.2	17.1	16.2	19.3	17.7	17.1	17.4
Zr	93.7	91.3	90.9	92.4	94.3	95.4	92.8	92.9	95.5	98.1	94.6	93.6	96.6	97.3	99.1	97.4	96.1	98.9	100.5	101.3
Nb	4.1	3.9	4.4	4.7	3.9	5.0	4.6	4.9	4.2	5.2	5.4	4.5	4.9	5.2	5.6	5.5	5.8	6.0	5.7	6.7
Zn	101.3	95.3	94.2	101.4	98.1	110.1	95.2	98.2	107.5	102.1	91.8	92.2	94.3	98.4	96.7	97.6	85.3	111.2	109.7	107.3
Ni	122.7	138.5	112.8	121.1	154.4	104.5	104.1	117.8	117.5	113.7	118.6	144.2	123.0	119.8	121.0	118.6	103.9	139.7	121.2	117.3
Cr	277.4	261.5	258.2	258.3	242.0	256.1	233.6	240.9	238.6	240.9	221.4	214.1	222.3	236.2	235.3	232.3	217.2	222.8	215.1	233.7
V	352.0	346.6	339.1	348.9	339.1	349.2	340.8	338.4	339.1	360.2	335.2	325.9	340.2	349.4	346.7	346.0	383.7	362.1	371.3	365.3
Mg′-value	0.54	0.59	0.59	0.57	0.63	0.58	0.58	0.58	0.58	0.55	0.57	0.60	0.58	0.58	0.57	0.58	0.47	0.56	0.54	0.54
FeO*	10.39	10.16	10.42	10.44	9.10	10.54	10.73	10.64	11.13	10.67	10.67	11.08	10.75	10.76	10.40	10.71	11.76	10.81	11.28	11.30
CaO/Al_2O_3	0.81	0.80	0.79	0.80	0.79	0.80	0.79	0.78	0.78	0.78	0.78	0.78	0.79	0.79	0.79	0.78	0.91	0.78	0.79	0.79
Zr/Nb	22.9	23.4	20.7	19.7	24.2	19.1	20.2	19.0	22.7	18.9	17.5	20.8	19.7	18.7	17.7	17.7	16.6	16.5	17.6	15.1
Zr/Y	2.96	2.83	2.86	2.86	2.80	2.91	2.86	2.88	2.92	2.92	2.83	2.93	2.93	2.92	2.90	3.00	2.70	2.96	2.95	3.00

Note: See note at beginning of Appendix A. All samples belong to Chemical Group I.

APPENDIX B
Average Compositions of Basalts from Leg 82

Note to Appendix B tables: N refers to number of samples in each chemical group. Fe_2O_3* and FeO* refer to total Fe expressed as Fe^{3+} or Fe^{2+}. Calculation of Mg′-value is discussed in the text (Mg/[Mg + Fe^2]). Small discrepancies in totals may be attributed to rounding.

Table 1. Hole 556.

Chemical group	I	IA	IB	II
N	12	9	3	4
Major elements (wt.%)				
SiO_2	50.11	50.27	50.06	50.23
TiO_2	0.90	1.02	0.86	1.45
Al_2O_3	15.99	15.94	16.49	15.95
Fe_2O_3*	8.40	9.12	8.16	10.73
MnO	0.15	0.15	0.14	0.17
MgO	7.44	7.43	7.53	6.75
CaO	13.26	13.16	14.23	11.71
Na_2O	2.35	2.36	2.34	2.74
K_2O	0.33	0.34	0.25	0.27
P_2O_5	0.11	0.11	0.11	0.15
Total	99.04	99.90	100.17	100.16
Trace elements (ppm)				
Rb	6.4	7.3	3.3	4.7
Sr	99	99	100	100
Y	22.4	22.7	19.6	31.8
Ga	15.1	15.2	14.3	16.6
Zr	48.4	58.5	48.4	92.8
Nb	1.8	1.7	2	2.5
Zn	73	73	71	90
Ni	100	99	111	89
Cr	340	342	319	250
V	229	230	218	248
Mg′-value	0.66	0.64	0.67	0.58
FeO*	8.17	8.25	7.34	9.66
CaO/Al_2O_3	0.83	0.83	0.87	0.73
Zr/Nb	33.7	36.4	24.6	37.8
Zr/Y	2.57	2.58	2.57	2.92

Note: See note at beginning of Appendix B.

Table 2. Hole 558.

Chemical group	I	II	III	IIIA	IIIB	IV
N	3	1	7	1	6	5
Major elements (wt.%)						
SiO_2	49.75	51.09	50.27	50.32	50.22	49.28
TiO_2	1.26	1.16	1.35	1.45	1.31	0.99
Al_2O_3	15.07	15.82	15.14	15.16	15.11	16.05
Fe_2O_3*	10.30	8.80	10.11	10.46	9.75	10.06
MnO	0.17	0.16	0.16	0.15	0.16	0.16
MgO	8.76	8.26	8.52	8.17	8.86	8.90
CaO	11.67	12.40	11.63	11.58	11.67	12.11
Na_2O	2.34	2.15	2.22	2.30	2.13	2.12
K_2O	0.36	0.17	0.41	0.46	0.35	0.26
P_2O_5	0.17	0.12	0.20	0.21	0.18	0.13
Total	99.85	100.14	100.01	100.27	99.75	100.06
Trace elements (ppm)						
Rb	5.8	2.5	8.20	9.7	6.7	4.9
Sr	139	95	173	170	176	112
Y	22.9	25.6	22.8	24.2	21.45	18.7
Ga	15.3	16.0	15.4	15.6	15.2	14.8
Zr	79.2	66.5	87.6	92.8	82.3	56.2
Nb	9.8	3.1	14.4	15.2	13.6	7.5
Zn	87.2	90	88	89	87	79
Ni	169	170	160	157	162	205
Cr	344	400	368	356	379	461
V	243	238	250	259	243	203
Mg′-value	0.65	0.68	0.66	0.64	0.67	0.66
FeO*	9.27	7.92	9.10	9.41	8.79	9.05
CaO/Al_2O_3	0.78	0.78	0.77	0.77	0.77	0.76
Zr/Nb	8.10	21.46	6.08	6.09	6.06	7.45
Zr/Y	3.46	2.60	3.83	3.83	3.83	3.00

Note: See note at beginning of Appendix B.

Table 3. Hole 559.

Chemical group	I
N	9
Major elements (wt.%)	
SiO_2	49.52
TiO_2	1.54
Al_2O_2	15.46
Fe_2O_3*	10.97
MnO	0.17
MgO	7.11
CaO	11.73
Na_2O	2.58
K_2O	0.47
P_2O_5	0.21
Total	99.77
Trace elements (ppm)	
Rb	8.1
Sr	165
Y	28.3
Ga	16.0
Zr	106.9
Nb	15.0
Zn	103
Ni	135
Cr	258
V	267
Mg'-value	0.59
FeO*	9.88
CaO/Al_2O_3	0.76
Zr/Nb	7.09
Zr/Y	3.78

Note: See note at beginning of Appendix B.

Table 4. Hole 561.

Chemical group	I	II
N	2	7
Major elements (wt.%)		
SiO_2	49.73	50.15
TiO_2	1.22	1.36
Al_2O_3	15.38	14.99
Fe_2O_3*	9.92	11.45
MnO	0.16	0.18
MgO	8.06	7.44
CaO	12.21	11.58
Na_2O	2.50	2.54
K_2O	0.36	0.36
P_2O_5	0.23	0.13
Total	99.75	100.18
Trace elements (ppm)		
Rb	5.5	8.3
Sr	215	89
Y	25.5	31.7
Ga	15.2	17.4
Zr	100.9	74.4
Nb	21.7	2.7
Zn	69	102
Ni	176	130
Cr	414	232
V	238	301
Mg'-value	0.64	0.59
FeO*	8.92	10.30
CaO/Al_2O_3	0.80	0.77
Zr/Nb	4.65	28.5
Zr/Y	3.95	2.34

Note: See note at beginning of Appendix B.

Table 5. Hole 562.

Chemical group	I	II
N	6	10
Major elements (wt.%)		
SiO_2	49.69	49.43
TiO_2	1.57	1.23
Al_2O_3	15.59	16.38
Fe_2O_3*	11.49	10.21
MnO	0.18	0.16
MgO	7.03	7.23
CaO	11.64	12.87
Na_2O	2.52	2.06
K_2O	0.23	0.25
P_2O_5	0.16	0.13
Total	100.10	99.95
Trace elements (ppm)		
Rb	3.9	4.6
Sr	100	98
Y	34.2	27.1
Ga	17.5	16.2
Zr	95.7	70.2
Nb	3.4	2.6
Zn	96	88
Ni	109	108
Cr	231	256
V	291	262
Mg'-value	0.57	0.61
FeO*	10.34	9.11
CaO/Al_2O_3	0.74	0.79
Zr/Nb	28.2	27.8
Zr/Y	2.76	2.59

Note: See note at beginning of Appendix B.

Table 6. Hole 563.

Chemical group	I
N	8
Major elements (wt.%)	
SiO_2	49.69
TiO_2	1.00
Al_2O_3	15.90
Fe_2O_3*	10.11
MnO	0.16
MgO	7.67
CaO	13.08
Na_2O	2.08
K_2O	0.27
P_2O_5	0.10
Total	100.06
Trace elements (ppm)	
Rb	5.6
Sr	84
Y	23.4
Ga	15.4
Zr	55.9
Nb	2.3
Zn	81
Ni	103
Cr	329
V	292
Mg'-value	0.63
FeO*	9.16
CaO/Al_2O_3	0.82
Zr/Nb	24.6
Zr/Y	2.39

Note: See note at beginning of Appendix B.

Table 7. Hole 564.

Chemical group	I
N	
Major elements (wt.%)	
SiO_2	49.69
TiO_2	1.48
Al_2O_3	14.89
Fe_2O_3	11.87
MnO	0.18
MgO	7.16
CaO	11.85
Na_2O	2.38
K_2O	0.35
P_2O_5	0.16
Total	100.01
Trace elements (ppm)	
Rb	6.1
Sr	105
Y	33.0
Ga	17.1
Zr	95.6
Nb	5.0
Zn	99
Ni	117
Cr	238
V	349
Mg'-value	0.57
FeO*	10.69
CaO/Al_2O_3	0.80
Zr/Nb	19.4
Zr/Y	2.90

Note: See note at beginning of Appendix B.